

Importance of vector leptoquark-scalar box diagrams in Pati-Salam unification with vector-like families

Syuhei Iguro^{1,2}, Junichiro Kawamura³, Shohei Okawa⁴, and Yuji Omura⁵

¹*Institute for Theoretical Particle Physics (TTP), Karlsruhe Institute of Technology (KIT), Engesserstraße 7, 76131 Karlsruhe, Germany*

²*Institute for Astroparticle Physics (IAP), Karlsruhe Institute of Technology (KIT), Hermann-von-Helmholtz-Platz 1, 76344 Eggenstein-Leopoldshafen, Germany*

³*Center for Theoretical Physics of the Universe, Institute for Basic Science (IBS), Daejeon 34051, Korea*

⁴*Departament de Física Quàntica i Astrofísica, Institut de Ciències del Cosmos (ICCUB), Universitat de Barcelona, Martí i Franquès 1, E-08028 Barcelona, Spain*

⁵*Department of Physics, Kindai University, Higashi-Osaka, Osaka 577-8502, Japan*

Abstract

We study lepton flavor violation (LFV) induced by one-loop box diagrams in Pati-Salam (PS) unification with vector-like families. The vector leptoquark (LQ) associated with the PS gauge symmetry breaking generally causes various LFV processes such as $K_L \rightarrow \mu e$ and $\mu \rightarrow e$ conversion at the tree-level, thereby driving its mass scale to be higher than PeV scale. The vector-like families are introduced to suppress such tree-level LFV processes, allowing the LQ to have TeV scale mass. In this paper, we point out that there are inevitable one-loop contributions to those LFV processes from the box diagrams mediated by both one LQ and one scalar field, even if the tree-level contributions are suppressed. We consider a concrete model for demonstration, and show that the vector-like fermion masses have an upper bound for a given LQ mass when the one-loop induced processes are consistent with the experimental limits. The vector-like fermion mass should be lighter than 3 TeV for 20 TeV LQ, if a combination of the couplings does not suppress $K_L \rightarrow \mu e$ decay. Our findings would illustrate importance of the box diagrams involving both LQ and physical modes of symmetry breaking scalars in TeV scale vector LQ models.

KEYWORDS: Pati-Salam, Vector leptoquark, Box diagrams, Lepton flavor violation

Contents

1	Introduction	2
2	Pati-Salam model with TeV-scale vector LQ	3
2.1	Minimal Pati-Salam model	3
2.2	Schematic picture of tree-level flavor violation	4
2.3	Schematic picture of loop-level flavor violation	5
2.4	Realistic model	6
2.5	Mass matrix	6
2.6	Couplings with the vector LQ and scalars	8
3	Flavor violations from box diagrams	10
3.1	Tree-level constraints	10
3.2	Box contributions	11
4	Phenomenology	15
4.1	Flavor violating leptonic decays of neutral mesons	15
4.2	μ - e conversion	17
4.3	Simplified analysis	18
4.4	Comments on penguin diagrams	22
5	Summary	24
A	Loop functions	25
B	Tree-level constraints	26

1 Introduction

The Pati-Salam (PS) unification [1] is a compelling new physics scenario, given an ambitious motivation as a potential pathway toward grand unified theories. In recent years, with growing interests in empirical hints for new physics found in flavor violating observables, significant attention has been paid to PS models and their variants with TeV scale symmetry breaking. Indeed, a vector leptoquark (LQ), appearing as a result of the PS symmetry breaking, has the same quantum number as a well-studied single mediator solution to the $R_{K^{(*)}}$ [2–10] and $R_{D^{(*)}}$ [11–20] anomalies. Furthermore, such a particle could also account for the muon $g - 2$ anomaly [21–25].

In the basic construction of the PS unification, there are two known difficulties in lowering the PS symmetry breaking scale. Firstly, PS models partly unify quarks and leptons and hence predict the common mass matrices to them, which obviously contradicts the observed fermion spectra. Secondly, the vector LQ associated with the symmetry breaking carries both baryon and lepton numbers and couples quarks and leptons flavor-dependently at the tree-level. These couplings easily induce various flavor violating processes that are suppressed in the Standard Model (SM) [26]. In the conventional setup, the $K_L \rightarrow \mu e$ decay brings the most severe limit and pushes the PS breaking scale to be heavier than 1 PeV [27, 28].

In recent studies, mainly stimulated by the B meson anomalies, it has been shown that both problems can be resolved by introducing vector-like fermions mixed with the SM chiral fermions [29–31]. When specific relations between PS conserving vector-like masses and those originated from PS breaking are imposed, the vector LQ does not couple to a SM lepton and quark simultaneously and thus the serious lepton flavor violating (LFV) processes are absent at the tree-level, thereby allowing the TeV scale LQ. This solution, however, relies on a 0.1% level tuning between the PS conserving and breaking masses to be consistent with the strong flavor constraints [31]. We emphasize that the cancellations at the tree-level are not ensured by any symmetry, and thus loop-corrections possibly induce flavor violating processes in these models.

Loop-induced flavor violations in new physics models with LQs have been studied in connection with the B anomalies, e.g. based on a PS model [29], 4321 models [32, 33], extra dimension model [34] and composite model [35].¹ In these works, it turns out that the $b \rightarrow c$ transition correlates with the B_s mixing induced by box diagrams with two LQs or two scalars. The $R_{D^{(*)}}$ anomaly can be explained consistently only when the Glashow-Iliopoulos-Maiani (GIM) like mechanism [37] works for those box diagrams.

In this paper, we study another class of box diagrams which involve one vector LQ and one scalar, and evaluate how such diagrams impact on the LFV processes. As a demonstration, we consider a simple PS model only with vector-like copies of the SM chiral fermions and an $SU(4)_C$ adjoint scalar field in addition to the three generations of chiral fermions². In this setup, we compute all box diagrams relevant to the flavor violating processes associated with down-type quarks and charged leptons. Although several types of the Wilson coefficients turn out to be

¹See also Ref. [36].

²Additional scalar fields are necessary to break the residual $SU(2)_R \times U(1)_{B-L}$ gauge symmetry as well as generating neutrino masses and mixings via the see-saw mechanism. We do not discuss its explicit realization since this would not affect the flavor violations discussed in this work. An explicit model with $(\overline{\mathbf{10}}, \mathbf{1}, \mathbf{3})$ is studied in Ref. [31].

Table 1: The matter content in the Pati-Salam model.

fields	spin	$SU(4)_C$	$SU(2)_L$	$SU(2)_R$
L	1/2	4	2	1
F_L	1/2	4	2	1
F_R	1/2	4	2	1
R	1/2	4	1	2
f_R	1/2	4	1	2
f_L	1/2	4	1	2
Δ	0	15	1	1
Φ	0	1	2	$\bar{\mathbf{2}}$

cancelled due to the GIM-like mechanism, we shall find that such cancellation does not work for contributions originated from box diagrams involving both LQ and PS breaking scalar. These contributions, thus, induce the LFV processes which are severely constrained. We also observe that the unsuppressed pieces are proportional to the powers of the ratio of the vector-like fermion mass to the LQ mass. This indicates that the vector-like fermion masses are constrained from above for a given LQ mass. Interestingly, the vector-like fermions have to reside at the TeV scale or below if the PS symmetry breaks down at the TeV scale, which is suggested by the anomalies of the B -meson decays.

This paper is organized as follows. In Sec. 2, we introduce our PS model and explain how the observed mass spectra are realized by introducing vector-like fermions in addition to chiral ones. We also schematically explain how the box diagrams involving both LQ and scalar can induce sizable LFV processes. In Sec. 3, the box-induced contributions to the semi-leptonic operators are evaluated and the non-vanishing coupling structures are identified. We perform numerical analysis of the one-loop contributions in Sec. 4 and discuss the impact on the PS model construction. Section 5 is devoted to summary.

2 Pati-Salam model with TeV-scale vector LQ

2.1 Minimal Pati-Salam model

We consider a model with the PS gauge symmetry, $SU(4)_C \times SU(2)_L \times SU(2)_R$. The PS symmetry identifies the lepton number as a fourth color of $SU(4)_C$, and SM chiral quark and lepton fields in the same $SU(2)_L$ representation are unified into chiral fields, L_i and R_i ($i = 1, 2, 3$), whose representations are respectively $(\mathbf{4}, \mathbf{2}, \mathbf{1})$ and $(\mathbf{4}, \mathbf{1}, \mathbf{2})$ under the PS symmetry. The electroweak (EW) doublet Higgs fields are embedded in a bi-doublet field of $SU(2)_L \times SU(2)_R$, Φ , whose representation is $(\mathbf{1}, \mathbf{2}, \bar{\mathbf{2}})$. With this minimal content, the general Yukawa interaction is given by

$$-\mathcal{L}_Y^{\min} = \bar{L}Y_1\Phi R + \bar{L}Y_2\epsilon^T\Phi^*\epsilon R + h.c., \quad (2.1)$$

where $\epsilon := i\sigma_2$ acts on the $SU(2)_L$ and $SU(2)_R$ indices and Y_1 and Y_2 are 3×3 Yukawa matrices in the flavor space. A massive vector LQ, X^μ , appears as a result of the $SU(4)_C \rightarrow SU(3)_C \times U(1)_{B-L}$ breaking. The LQ interaction is in the form of

$$\mathcal{L}_X = \frac{g_4}{\sqrt{2}} X_\mu \left(\bar{d}_L^i \gamma^\mu e_L^i + \bar{u}_L^i \gamma^\mu \nu_L^i + \bar{d}_R^i \gamma^\mu e_R^i + \bar{u}_R^i \gamma^\mu \nu_R^i \right) + h.c., \quad (2.2)$$

which is written in the flavor basis and hence diagonal and universal unless the $SU(4)_C$ breaking effects to the fermion masses are taken into account. The CKM mixing factors will appear in the left-handed fermion interactions once we move to the mass basis. The interaction terms in Eqs. (2.1) and (2.2) explicitly show two problems inherent in the minimal PS model. One is that the minimal Yukawa terms in Eq. (2.1) predict the same mass matrices for quarks and leptons, i.e. $m_e^{ij} = m_d^{ij}$ and $m_u^{ij} = m_\nu^{ij}$. The other is that the LQ interaction in Eq. (2.2) mediates $\bar{d}_i d_j \rightarrow \bar{e}_i e_j$ processes at the tree-level and triggers the rapid LFV processes, e.g. $K_L \rightarrow \mu e$.

2.2 Schematic picture of tree-level flavor violation

These problems can be resolved by introducing $SU(4)_C$ charged scalar fields and vector-like fermions in addition to L^i and R^i . Before proceeding to the general argument, we briefly demonstrate our basic idea to create the mass splitting with a particular focus on the down-type quarks and charged leptons. The up-type quark and neutrino masses can be realized independently of the discussion below. For a demonstrative purpose, we only focus on a single generation of L^i and add one vector-like copy $F_{L,R} = (\mathbf{4}, \mathbf{2}, \mathbf{1})$ and an $SU(4)_C$ adjoint scalar field Δ [29, 31]. With this extended content, we can write down additional interaction terms,

$$-\mathcal{L}_M = \bar{L} (m_L + \kappa_L \Delta) F_R + \bar{F}_L (M_L + Y_L \Delta) F_R + h.c., \quad (2.3)$$

where m_L and M_L are the PS symmetric mass parameters. Decomposing the fermions

$$L = \begin{pmatrix} \nu_L & e_L \\ u_L & d_L \end{pmatrix}, \quad F_A = \begin{pmatrix} N_A & E_A \\ U_A & D_A \end{pmatrix}, \quad (2.4)$$

with $A = L, R$ and after the adjoint field develops the vacuum expectation value (VEV) $\langle \Delta \rangle = v_\Delta / (2\sqrt{3}) \text{diag}(3, -1, -1, -1)$, the mass terms take the form of

$$\begin{aligned} -\mathcal{L}_M &= \bar{d}_L \left(m_L - \frac{\kappa_L v_\Delta}{2\sqrt{3}} \right) D_R + \bar{D}_L \left(M_L - \frac{Y_L v_\Delta}{2\sqrt{3}} \right) D_R \\ &+ \bar{e}_L \left(m_L + \frac{3\kappa_L v_\Delta}{2\sqrt{3}} \right) E_L + \bar{E}_L \left(M_L + \frac{3Y_L v_\Delta}{2\sqrt{3}} \right) E_R + \dots, \end{aligned} \quad (2.5)$$

where we only show the down-type quarks and charged leptons explicitly. When the cancellation conditions,

$$m_L - \frac{\kappa_L v_\Delta}{2\sqrt{3}} = 0, \quad M_L + \frac{3Y_L v_\Delta}{2\sqrt{3}} = 0, \quad (2.6)$$

are imposed, it follows that only (D_L, D_R) and (e_L, E_R) have vector-like masses,

$$-\mathcal{L}_M = \left(M_L - \frac{Y_L v_\Delta}{2\sqrt{3}} \right) \overline{D}_L D_R + \left(m_L + \frac{3\kappa_L v_\Delta}{2\sqrt{3}} \right) \overline{e}_L E_R + \dots, \quad (2.7)$$

whereas d_L and E_L remain massless which are identified as the SM fermions. These massless quark and lepton respectively originate in the different PS multiplets, L and F_L . This indicates that unlike the minimal model, they have different Yukawa couplings to the bi-doublet scalar Φ , which in turn results in different mass matrices for the quark and lepton after the EW symmetry breaking. The left-handed LQ couplings are now in the form of

$$\mathcal{L}_X = \frac{g_4}{\sqrt{2}} X_\mu (\overline{d}_L \gamma^\mu e_L + \overline{D}_L \gamma^\mu E_L) + \dots. \quad (2.8)$$

Since e_L and D_L are heavy, the LQ coupling always involves heavy fermions, not mediating the LFV meson decays at the tree-level. It should be noted that the EW gauge interactions remain unchanged under this exchange of the $SU(2)_L$ doublets e_L and E_L . The mass splitting of the right-handed quark and lepton can be realized by introducing a corresponding vector-like copy in an analogous way.

2.3 Schematic picture of loop-level flavor violation

Now we have seen that the mass splittings are generated by introducing the vector-like fermions. Following this method and adding more vector-like families, we can realize the observed mass spectra and well suppress the tree-level LFV processes in the three-generation case [31]. On the other hand, this trick predicts a specific interaction structure that will revive the LFV processes via one-loop box diagrams. To see this, we explicitly keep the radial mode of Δ by the replacement $v_\Delta \rightarrow v_\Delta + h_\Delta$ in Eq. (2.5). We then obtain Yukawa interactions of h_Δ ,

$$-\mathcal{L}_M = -\frac{\kappa_L}{2\sqrt{3}} h_\Delta \overline{d}_L D_R + \frac{3Y_L}{2\sqrt{3}} h_\Delta \overline{E}_L E_R + \dots. \quad (2.9)$$

Although there is no mass term in the form of $\overline{d}_L D_R$ and $\overline{E}_L E_R$, the couplings of $h_\Delta \overline{d}_L D_R$ and $h_\Delta \overline{E}_L E_R$ are present. Thus, the $d \rightarrow e$ transition arises via the interaction to the radial mode h_Δ ,

$$\frac{g_4 \kappa_L}{2\sqrt{6} M_D} h_\Delta X_\mu \overline{d}_L \gamma^\mu E_L, \quad (2.10)$$

where we assume the vector-like fermions are heavy and integrate them out (see also Fig. 1). We note that E_L is a SM-like lepton. Further integrating out the LQ and h_Δ , we will obtain semi-leptonic operators that give rise to various LFV processes such as $K_L \rightarrow \mu e$ and $\mu \rightarrow e$ conversion.

One may wonder if other box diagrams involving two LQs or two h_Δ scalars can also induce the same semi-leptonic operators. This is true indeed, but as we will show in the rest of this paper, such contributions can be suppressed by the GIM-like mechanism. On the contrary, the LQ-scalar box contributions via the combination of Eqs. (2.8) and (2.9) have no such suppression and thus are unavoidable. The evaluation of the LQ-scalar box diagrams is the main aim of this paper. In the following, we will study a realistic version of the PS extension highlighted above and perform analytical and numerical analyses to derive quantitative limits on the model.

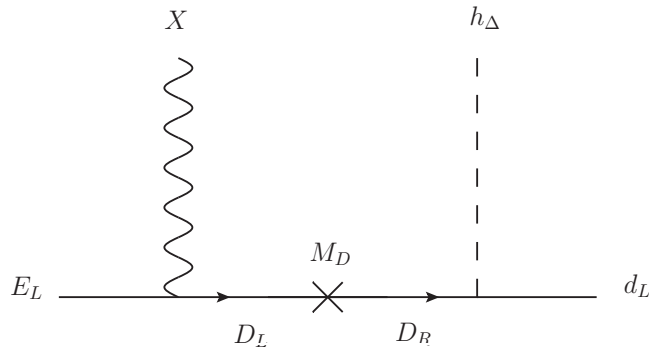


Figure 1: A schematic picture of regenerating the $d \rightarrow e$ transition via the interaction to the radial mode of the PS symmetry breaking scalar h_Δ .

2.4 Realistic model

In this section, we generalize the above discussion to accommodate the realistic quark and lepton masses. The matter contents of the model is summarized in Table 1. We introduce N_L vector-like $SU(2)_L$ doublet fermions $F_{L,R}$ and N_R vector-like $SU(2)_L$ singlet fermions $f_{L,R}$ in addition to L^i , R^i and Φ . Here F_L and f_R possess the same quantum numbers as those of L and R , respectively, and F_R and f_L are their vector-like pairs. The relevant part of Lagrangian is given by

$$-\mathcal{L}_M = \bar{F}_L (M_L + Y_L \Delta) F_R + \bar{L} (m_L + \kappa_L \Delta) F_R + \bar{f}_L (M_R + Y_R \Delta) f_R + \bar{f}_L (m_R + \kappa_R \Delta) R + \dots, \quad (2.11)$$

where all couplings and masses are considered as matrices in the flavor space and the ellipsis represents the interactions between the fermions and the Higgs bi-doublet field Φ . The fermions are decomposed into quarks and leptons as

$$L = \begin{pmatrix} \nu_L & e_L \\ u_L & d_L \end{pmatrix}, \quad R = \begin{pmatrix} \nu_R & e_R \\ u_R & d_R \end{pmatrix}, \quad F_A = \begin{pmatrix} N_A & E_A \\ U_A & D_A \end{pmatrix}, \quad f_A = \begin{pmatrix} \mathcal{N}_A & \mathcal{E}_A \\ \mathcal{U}_A & \mathcal{D}_A \end{pmatrix}, \quad (2.12)$$

where the index $A = L, R$ represents the chirality. The scalar fields obtain non-vanishing VEVs,

$$\langle \Delta \rangle = \frac{v_\Delta}{2\sqrt{3}} \begin{pmatrix} 3 & 0 \\ 0 & -\mathbf{1}_3 \end{pmatrix}, \quad \langle \Phi \rangle = v_H \begin{pmatrix} \cos \beta & 0 \\ 0 & \sin \beta \end{pmatrix}. \quad (2.13)$$

2.5 Mass matrix

We shall see the mass mixing of the fermions, which is directly linked to the coupling structure of the LQ and scalars. We mainly discuss the flavor violating processes among the down-type quarks and charged leptons in this paper, so that we only show the relevant terms.³ Without loss

³See Ref. [31] for the full detail of the mass mixing and diagonalization including the up-type quarks and neutrinos.

of generality, the fermion mass terms are given by

$$\begin{aligned}
-\mathcal{L}_{\text{mass}} &= \bar{\mathbf{d}}_L \mathcal{M}_d \mathbf{d}_R + \bar{\mathbf{e}}_L \mathcal{M}_e \mathbf{e}_R \\
&:= \begin{pmatrix} \bar{d}_L \\ \bar{D}_L \\ \bar{\mathcal{D}}_L \end{pmatrix}^T \begin{pmatrix} m_{33} & m_{3R} & 0_{3 \times N_L} \\ m_{L3} & m_{LR} & D_{d_L} \\ 0_{N_R \times 3} & D_{d_R} & m_{RL} \end{pmatrix} \begin{pmatrix} d_R \\ \mathcal{D}_R \\ D_R \end{pmatrix} + \begin{pmatrix} \bar{e}_L \\ \bar{E}_L \\ \bar{\mathcal{E}}_L \end{pmatrix}^T \begin{pmatrix} m_{33} & m_{3R} & M_{eE} \\ m_{L3} & m_{LR} & M_{EE} \\ M_{\mathcal{E}e} & M_{\mathcal{E}E} & m_{RL} \end{pmatrix} \begin{pmatrix} e_R \\ \mathcal{E}_R \\ E_R \end{pmatrix}
\end{aligned} \tag{2.14}$$

where D_{d_A} is an $N_A \times N_A$ diagonal matrix and $m_{\alpha\beta}$ ($\alpha, \beta = 3, L, R$) is an $N_\alpha \times N_\beta$ mass matrix of $\mathcal{O}(v_H)$. Here, $N_\alpha = 3$ for $\alpha = 3$. Note that the structure of $m_{\alpha\beta}$ is common to \mathcal{M}_d and \mathcal{M}_e due to the PS symmetry. We define the mass basis for the fermions as

$$\hat{\mathbf{d}}_A = U_{d_A}^\dagger \mathbf{d}_A, \quad \hat{\mathbf{e}}_A = U_{e_A}^\dagger \mathbf{e}_A. \tag{2.15}$$

The unitary matrices, U_{f_A} ($f = e, d$), diagonalize the mass matrices as

$$U_{f_L}^\dagger \mathcal{M}_f U_{f_R} = \text{diag} \left(m_1^f, m_2^f, m_3^f, \dots, m_{N_L+N_R+3}^f \right). \tag{2.16}$$

The three lightest fermions correspond to the SM fermions and there are $N_L + N_R$ extra fermions.

We are interested in the approximate forms of the unitary matrices with $\eta := m_{\alpha\beta}/v_\Delta \ll 1$ ⁴. Hence we only keep the leading contribution by neglecting $\mathcal{O}(\eta)$ corrections. Assuming the elements of D_{d_L} and D_{d_R} are larger than the other elements, the masses of the chiral three families (d_L, d_R) are mostly given by $m_{33} \sim \mathcal{O}(\eta)$. Then, (d_L, d_R) does not mix with the vector-like families at the leading order in η and can be regarded as SM-like. On the other hand, the charged leptons (e_L, e_R) do not correspond to the SM families due to the vector-like masses $M_{\mathcal{E}e}$ and M_{eE} . The vector-like masses for the charged leptons can be, in general, decomposed as

$$\begin{pmatrix} M_{eE} \\ M_{EE} \end{pmatrix} =: V_L \begin{pmatrix} D_{eL} \\ 0_{3 \times N_L} \end{pmatrix} W_R^\dagger, \quad \begin{pmatrix} M_{\mathcal{E}e} & M_{\mathcal{E}E} \end{pmatrix} =: W_L \begin{pmatrix} 0_{N_R \times 3} & D_{eR} \end{pmatrix} V_R^\dagger, \tag{2.17}$$

where D_{e_A} is a diagonal $N_A \times N_A$ matrix with real positive entries, V_A and W_A are $(3+N_A) \times (3+N_A)$ and $N_{\bar{A}} \times N_{\bar{A}}$ unitary matrices and \bar{A} denotes the opposite chirality of A (i.e. $\bar{A} = R, L$ for $A = L, R$). Hence, the unitary matrices are approximately given by

$$\begin{aligned}
U_{d_L} &= \begin{pmatrix} \mathbf{1}_3 & 0 & 0 \\ 0 & 0 & \mathbf{1}_{N_L} \\ 0 & \mathbf{1}_{N_R} & 0 \end{pmatrix}, & U_{d_R} &= \begin{pmatrix} \mathbf{1}_3 & 0 & 0 \\ 0 & \mathbf{1}_{N_R} & 0 \\ 0 & 0 & \mathbf{1}_{N_L} \end{pmatrix}, \\
U_{e_L} &= \begin{pmatrix} V_L & 0_{(3+N_L) \times N_R} \\ 0_{N_R \times (3+N_L)} & W_L \end{pmatrix} P, & U_{e_R} &= \begin{pmatrix} 0_{(3+N_R) \times N_L} & V_R \\ W_R & 0_{N_L \times (3+N_R)} \end{pmatrix} P,
\end{aligned} \tag{2.18}$$

⁴If the $\mathcal{O}(v_H)$ entries are at most the bottom quark mass, we find $\eta \lesssim 10^{-3}$ for $v_\Delta \sim 4$ TeV.

with

$$P := \begin{pmatrix} 0 & 0 & \mathbf{1}_{N_L} \\ \mathbf{1}_3 & 0 & 0 \\ 0 & \mathbf{1}_{N_R} & 0 \end{pmatrix}. \quad (2.19)$$

The matrix V_L (V_R) represents the mixing within the $SU(2)_L$ doublets (singlets) in the left-handed (right-handed) sectors, while the matrix W_L (W_R) is the mixing within the $SU(2)_L$ singlets (doublets) in the left-handed (right-handed) sector. The vanishing blocks of $U_{e_A} P^{-1}$ reflect the fact that the $SU(2)_L$ doublet and singlet do not mix each other without the VEV of Φ . These blocks have non-vanishing entries of $\mathcal{O}(\eta)$ in fact. With the unitary matrices U_{d_A} and U_{e_A} in this form, the mass matrices are approximately diagonalized as

$$U_{d_L}^\dagger \mathcal{M}_d U_{d_R} = \begin{pmatrix} m_{33} & m_{3R} & 0 \\ 0 & D_{d_R} & m_{RL} \\ m_{L3} & m_{LR} & D_{d_L} \end{pmatrix} =: D_d, \quad U_{e_L}^\dagger \mathcal{M}_e U_{e_R} = \begin{pmatrix} \tilde{m}_{33} & \tilde{m}_{3R} & 0 \\ 0 & D_{e_R} & \tilde{m}_{RL} \\ \tilde{m}_{L3} & \tilde{m}_{LR} & D_{e_L} \end{pmatrix} =: D_e, \quad (2.20)$$

where

$$V_L^\dagger \begin{pmatrix} m_{33} & m_{3R} \\ m_{L3} & m_{LR} \end{pmatrix} V_R =: \begin{pmatrix} \tilde{m}_{L3} & \tilde{m}_{LR} \\ \tilde{m}_{33} & \tilde{m}_{3R} \end{pmatrix}, \quad W_L^\dagger m_{RL} W_R =: \tilde{m}_{RL}. \quad (2.21)$$

Neglecting the sub-dominant effects suppressed by η , the mass matrices of the SM down-type quarks and charged leptons are determined by m_{33} and \tilde{m}_{33} , respectively. Their singular values should be consistent with the SM fermion masses. The other elements of $m_{\alpha\beta}$ and $\tilde{m}_{\alpha\beta}$ give only sub-dominant effects to the mixing matrices as far as the vector-like fermions are sufficiently heavier than the EW scale.

2.6 Couplings with the vector LQ and scalars

The $SU(4)_C$ gauge symmetry is broken by the VEV of the adjoint scalar Δ . The massive gauge boson X_μ associated with the $SU(4)_C \rightarrow SU(3)_c \times U(1)_{B-L}$ breaking arises as a vector LQ. If Δ is the only source of the $SU(4)_C$ symmetry breaking, the LQ mass, m_X is given by

$$m_X = \frac{2}{\sqrt{3}} g_4 v_\Delta, \quad (2.22)$$

where g_4 denotes the $SU(4)_C$ gauge coupling. This relation is modified if other scalars contribute to the $SU(4)_C$ breaking.

The LQ couplings are given by the gauge interactions of the LQ to the fermions

$$\begin{aligned} \mathcal{L}_X &= \frac{g_4}{\sqrt{2}} X^\mu \left(\bar{\mathbf{d}}_L \gamma_\mu \mathbf{e}_L + \bar{\mathbf{d}}_R \gamma_\mu \mathbf{e}_R \right) + h.c. \\ &= X^\mu \left(\bar{\hat{\mathbf{d}}}_L \hat{g}_L \gamma_\mu \hat{\mathbf{e}}_L + \bar{\hat{\mathbf{d}}}_R \hat{g}_R \gamma_\mu \hat{\mathbf{e}}_R \right) + h.c., \end{aligned} \quad (2.23)$$

where the LQ couplings in the mass basis are expressed in terms of the fermion mixing matrices,

$$\hat{g}_L = \frac{g_4}{\sqrt{2}}\Omega_L, \quad \hat{g}_R = \frac{g_4}{\sqrt{2}}\Omega_R, \quad \text{with} \quad \Omega_L := U_{d_L}^\dagger U_{e_L}, \quad \Omega_R := U_{d_R}^\dagger U_{e_R}. \quad (2.24)$$

For a practical purpose, it is useful to decompose the unitary matrices $V_{L,R}$ as

$$V_L =: \begin{pmatrix} V_{3L} & X_L \\ Y_L & V_{L3} \end{pmatrix}, \quad V_R =: \begin{pmatrix} X_R & V_{3R} \\ V_{R3} & Y_R \end{pmatrix}, \quad (2.25)$$

with which we find $\Omega_{L,R}$ to be

$$\Omega_L = \begin{pmatrix} X_L & 0 & V_{3L} \\ 0 & W_L & 0 \\ V_{L3} & 0 & Y_L \end{pmatrix}, \quad \Omega_R = \begin{pmatrix} X_R & V_{3R} & 0 \\ V_{R3} & Y_R & 0 \\ 0 & 0 & W_R \end{pmatrix}. \quad (2.26)$$

It should be noted that we neglected the $\mathcal{O}(\eta)$ contribution above. The 3×3 matrix X_A in V_A represents the overlap of the SM charged leptons \hat{e}_A^i with the first three PS multiplets L^i and R^i which the SM down-type quarks \hat{d}_A^i mostly originate in. Thus, it follows from Eq. (2.26) that X_A stands for the LQ couplings to two SM fermions. As a reminder, taking $X_A = 0$ corresponds to the exact cancellation in Eq. (2.6).

After the $SU(4)_C$ breaking, the adjoint scalar Δ is decomposed into a singlet scalar h_Δ and an $SU(3)_c$ adjoint scalar Δ_8 :

$$\Delta = \frac{1}{2\sqrt{3}} \left(v_\Delta + \frac{h_\Delta}{\sqrt{2}} \right) \begin{pmatrix} 3 & 0 \\ 0 & -\mathbf{1}_3 \end{pmatrix} + \begin{pmatrix} 0 & 0 \\ 0 & \Delta_8 \end{pmatrix}, \quad (2.27)$$

where $\mathbf{1}_n$ denotes an $n \times n$ identity matrix. The Yukawa couplings involving h_Δ and Δ_8 are given by

$$-\mathcal{L}_\Delta = \sum_{\mathbf{f}=\mathbf{d},\mathbf{e}} \sqrt{\frac{3}{8}} h_\Delta Q_{B-L}^{\mathbf{f}} \bar{\mathbf{f}}_L Y_\Delta \mathbf{f}_R + \Delta_8 \bar{\mathbf{d}}_L Y_\Delta \mathbf{d}_R + h.c., \quad (2.28)$$

where $Q_{B-L}^{\mathbf{d}} = -1/3$ and $Q_{B-L}^{\mathbf{e}} = +1$ are the $B-L$ charges. The Yukawa couplings in the mass basis are given by

$$\hat{Y}_\Delta^f = \left(U_L^f \right)^\dagger Y_\Delta U_R^f, \quad f = d, e. \quad (2.29)$$

There is a close relation between the Yukawa coupling matrices in the gauge basis and the fermion mass matrices,

$$Y_\Delta = \frac{\sqrt{3}}{2v_\Delta} (\mathcal{M}_e - \mathcal{M}_d). \quad (2.30)$$

Using this relation, the Yukawa matrices in the mass basis are expressed as

$$\hat{Y}_\Delta^e = \frac{\sqrt{3}}{2v_\Delta} \left(D_e - \Omega_L^\dagger D_d \Omega_R \right) + \mathcal{O}(\eta). \quad \hat{Y}_\Delta^d = \frac{\sqrt{3}}{2v_\Delta} \left(\Omega_L D_e \Omega_R^\dagger - D_d \right) + \mathcal{O}(\eta). \quad (2.31)$$

The flavor violating couplings are thus induced via

$$\Omega_L^\dagger D_d \Omega_R \sim \begin{pmatrix} 0 & 0 & V_{L3}^\dagger D_{dL} W_R \\ W_L^\dagger D_{dR} V_{R3} & W_L^\dagger D_{dR} Y_R & 0 \\ 0 & 0 & Y_L^\dagger D_{dL} W_R \end{pmatrix} + \mathcal{O}(m_{\alpha\beta}), \quad (2.32)$$

$$\Omega_L D_e \Omega_R^\dagger \sim \begin{pmatrix} 0 & 0 & V_{3L} D_{eL} W_R^\dagger \\ W_L D_{eR} V_{3R}^\dagger & W_L D_{eR} Y_R^\dagger & 0 \\ 0 & 0 & Y_L D_{eL} W_R^\dagger \end{pmatrix} + \mathcal{O}(m_{\alpha\beta}). \quad (2.33)$$

One can see that the tree-level couplings of h_Δ and Δ_8 to the SM families are suppressed by η .

3 Flavor violations from box diagrams

In this section, we look at box contributions to the flavor violating processes, using the LQ and scalar couplings to the fermions derived in the previous section.

3.1 Tree-level constraints

We first summarize the constraints set by considering only the tree-level LQ exchange, which motivate us to impose a primary suppression condition. It follows from Eq. (2.26) that the LQ couplings to the SM fermions are given by X_L and X_R . With these couplings, the tree LQ exchange induces the semi-leptonic operators in the form of

$$\mathcal{L}_{\text{eff}} = \frac{g_4^2}{2m_X^2} \sum_{A,B=L,R} (X_A)^{ik} (X_B^\dagger)^{lj} (\bar{d}_A^i \gamma^\mu e_A^k) (\bar{e}_B^l \gamma_\mu d_B^j), \quad (3.1)$$

leading to various LFV processes, e.g. $K_L \rightarrow \mu e$, $B_d \rightarrow \tau e$, $B_s \rightarrow \tau \mu$ and $\mu \rightarrow e$ conversion. We show in Appendix B a rough estimate of experimental bounds on X_L and X_R , assuming $m_X = 5 \text{ TeV}$ and $g_4 = 1$. This set of bounds suggests that if all elements of X_A have comparable size, each matrix element should satisfy

$$|(X_L)^{ij}|, |(X_R)^{ij}| \lesssim \mathcal{O}(10^{-3}). \quad (3.2)$$

This limit motivates us to impose a condition for the suppressed flavor violation:

- (i) $X_L = X_R = 0$.

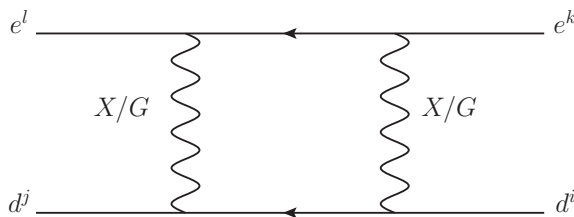


Figure 2: The box diagram involving LQ and Goldstone boson.

Given this condition, the unitarity of V_A requires that $N_A \geq 3$ and

$$V_{3A}V_{3A}^\dagger \simeq V_{A3}^\dagger V_{A3} \simeq \mathbf{1}_3. \quad (3.3)$$

Note that the exchange of h_Δ and Δ_8 does not cause any flavor violation at the tree-level, since their Yukawa couplings always contain the heavy fermions as seen in Eqs. (2.31), (2.32) and (2.33). Therefore, once the condition (i) is imposed, the model is free from the flavor violation at the tree-level.

3.2 Box contributions

We shall here look at box-diagram contributions to the semi-leptonic operators. Let us start with the box diagrams involving two LQs (Fig. 2). Under the condition (i), the LQ couplings to two SM fermions are vanishing (i.e. $X_A = 0$), so that we can only consider the vector-like fermions in the loop. In the diagrams where the internal fermion mass is not picked up, the external fermions maintain the chirality. Such contribution is given in the form of

$$(g_4)^4 \sum_{I,J \geq 4} f(m_I^e, m_J^d; m_X, m_X) [\Omega_A^\dagger]_{II} [\Omega_A]_{Ik} [\Omega_B]_{jJ} [\Omega_B^\dagger]_{Ji}, \quad (3.4)$$

where $A, B = L, R$ and $I, J = 4, 5, \dots, N_L + N_R + 3$ run only over the vector-like fermions. Given the unitarity of the LQ couplings Ω_A , this equation reminds us of the well-known GIM mechanism. Hence, we now suggest another suppression condition,

(ii) vector-like fermion masses are universal: $m_I^d =: m_D$ and $m_I^e =: m_E$ for $I \geq 4$.

This condition corresponds to $D_{d_L} \simeq m_D \mathbf{1}_{N_L}$, $D_{d_R} \simeq m_D \mathbf{1}_{N_R}$, $D_{e_L} \simeq m_E \mathbf{1}_{N_L}$ and $D_{e_R} \simeq m_E \mathbf{1}_{N_R}$ up to $\mathcal{O}(\eta)$ contributions. Under the conditions (i) and (ii), the loop function $f(m_I^e, m_J^d; m_X, m_X)$ can be pulled out of the summation over the internal fermion species and then we recognize the GIM-like suppression:

$$\sum_{I \geq 4} [\Omega_A^\dagger]_{II} [\Omega_A]_{Ik} \sim [V_{L3}^\dagger V_{L3}]_{Ik} \sim \delta_{Ik}, \quad (3.5)$$

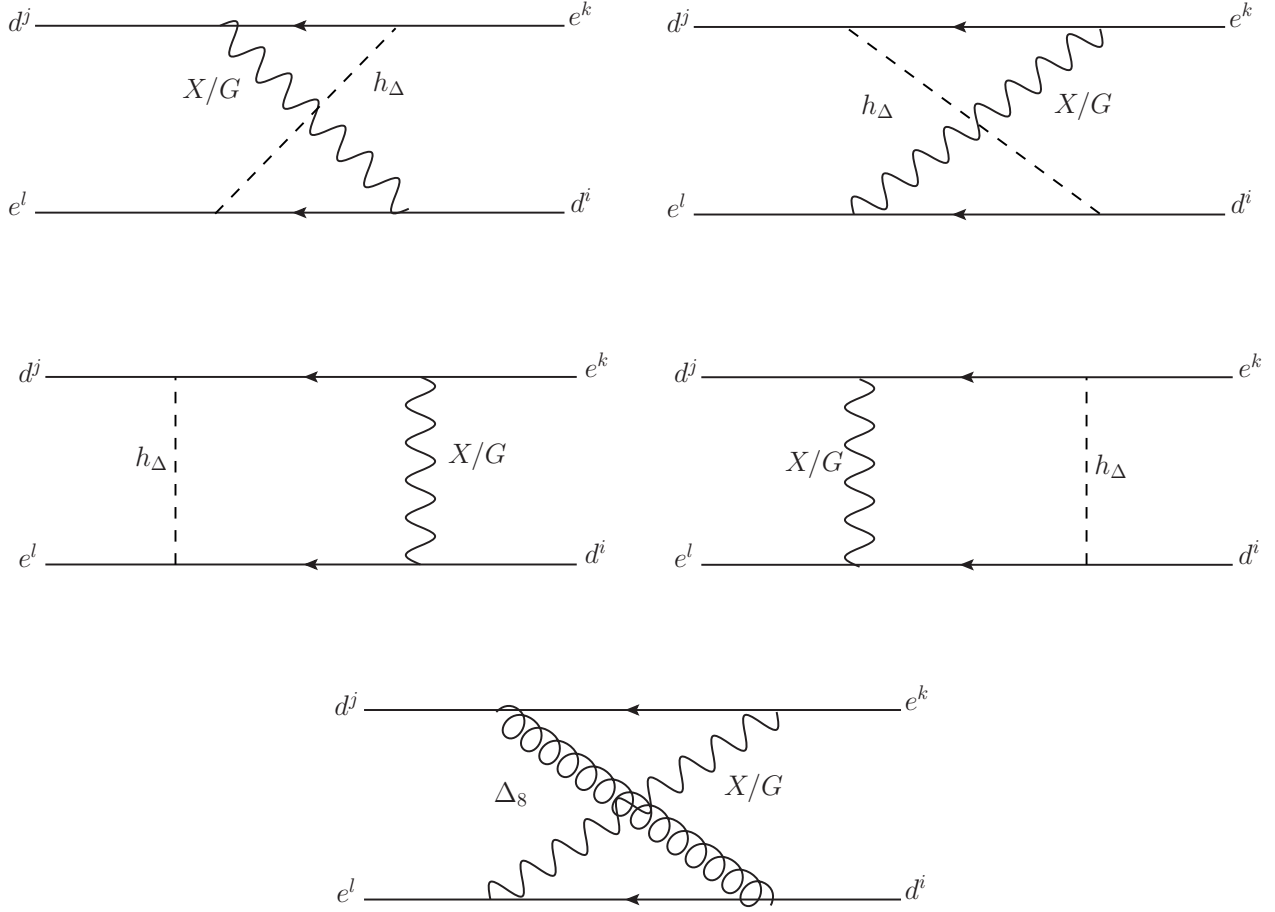


Figure 3: The box diagrams involving scalars and LQ/Goldstone.

where Eq. (3.3) is used. One can also show that the unitarity assures a similar suppression in the other combination $\sum_{J \geq 4} [\Omega_B]_{jJ} [\Omega_B^\dagger]_{Ji} \sim \delta_{ji}$. The flavor violating processes with $i \neq j$ or $k \neq l$ are therefore suppressed by the unitarity of Ω_A .

When the internal fermion mass is picked up, the chirality of the external fermions is flipped and different coupling combinations, e.g. $\Omega_L^\dagger D_d \Omega_R$, appear in the Wilson coefficients. Such contribution contains the factor,

$$m_D \sum_{I \geq 4} [\Omega_A^\dagger]_{II} [\Omega_{\bar{A}}]_{Ik} \sim 0, \quad (3.6)$$

where the condition (ii) is assumed. This result reflects the fact that there is no mixing between $SU(2)_L$ singlet and doublet fermions. Thus, any sizable flavor violation is not induced via the box diagram involving two LQs once the conditions (i) and (ii) are imposed.

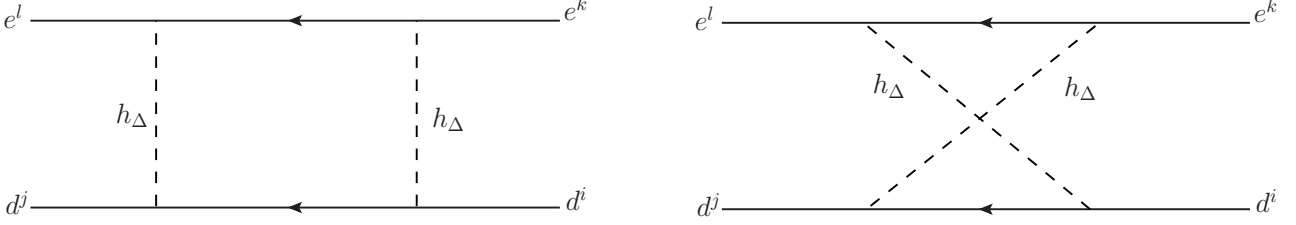


Figure 4: The box diagrams involving only scalars.

We next examine the box diagrams with h_Δ or Δ_8 in the loop. We have the diagrams involving one LQ and one scalar (Fig. 3) and the diagrams involving only scalars (Fig. 4). These diagrams generate the semi-leptonic operators,

$$\begin{aligned}
i\mathcal{L}_{\text{eff}} = & C_{VLL}^{ij,kl} \left(\bar{d}_L^j \gamma_\mu d_L^i \right) \left(\bar{e}_L^l \gamma_\mu e_L^k \right) + C_{VRR}^{ij,kl} \left(\bar{d}_R^j \gamma_\mu d_R^i \right) \left(\bar{e}_R^l \gamma_\mu e_R^k \right) \\
& + C_{VRL}^{ij,kl} \left(\bar{d}_R^j \gamma_\mu d_R^i \right) \left(\bar{e}_L^l \gamma_\mu e_L^k \right) + C_{VLR}^{ij,kl} \left(\bar{d}_L^j \gamma_\mu d_L^i \right) \left(\bar{e}_R^l \gamma_\mu e_R^k \right) \\
& + C_{SLL}^{ij,kl} \left(\bar{d}_R^j d_L^i \right) \left(\bar{e}_R^l e_L^k \right) + C_{SRR}^{ij,kl} \left(\bar{d}_L^j d_R^i \right) \left(\bar{e}_L^l e_R^k \right) \\
& + C_{SRL}^{ij,kl} \left(\bar{d}_L^j d_R^i \right) \left(\bar{e}_R^l e_L^k \right) + C_{SLR}^{ij,kl} \left(\bar{d}_R^j d_L^i \right) \left(\bar{e}_L^l e_R^k \right),
\end{aligned} \tag{3.7}$$

where the flavors of the quarks or leptons are different ($i \neq j$ or $k \neq l$). Under the conditions (i) and (ii) and assuming $m_{h_\Delta} = m_{\Delta_8}$ for simplicity, the Wilson coefficients are given by

$$C_{VAA}^{ij,kl} = \frac{3m_E^2 m_D^2}{8v_\Delta^4 m_X^2} \Upsilon_A^{li} \Upsilon_A^{*kj} \left[\frac{3}{16} G_1(m_E, m_D; m_X, m_{h_\Delta}) - \frac{g_4^2 v_\Delta^2}{m_X^2} G_0(m_E, m_D; m_X, m_{h_\Delta}) \right], \tag{3.8}$$

$$C_{V\bar{A}\bar{A}}^{ij,kl} = 0, \tag{3.9}$$

$$C_{SAA}^{ij,kl} = \frac{9m_E^3 m_D^3}{512v_\Delta^4 m_X^4} \Psi_A^{lk} \bar{\Psi}_A^{ji} \tilde{F}_0(m_E, m_D; m_{h_\Delta}, m_{h_\Delta}), \tag{3.10}$$

$$\begin{aligned}
C_{S\bar{A}\bar{A}}^{ij,kl} = & \frac{3m_E^2 m_D^2}{4v_\Delta^4 m_X^2} \Upsilon_A^{li} \Upsilon_A^{*kj} \left[-\frac{3}{16} G_1(m_E, m_D; m_X, m_{h_\Delta}) + \frac{g_4^2 v_\Delta^2}{m_X^2} G_0(m_E, m_D; m_X, m_{h_\Delta}) \right] \\
& + \frac{m_E^3 m_D^3}{8v_\Delta^4 m_X^4} \Psi_A^{lk} \bar{\Psi}_A^{*ji} \tilde{F}_0(m_E, m_D; m_{h_\Delta}, m_{h_\Delta}),
\end{aligned} \tag{3.11}$$

where the loop functions \tilde{F}_0, G_0 and G_1 are defined in Appendix A. The diagrams with one LQ and one scalar contribute to C_{VAA} and $C_{S\bar{A}\bar{A}}$, while the diagrams with two h_Δ contribute to C_{SAA} and $C_{S\bar{A}\bar{A}}$. Note that the box diagrams involving one LQ and one Goldstone boson are vanishing because of the GIM-like suppression.

The box contributions are expressed in terms of the combinations of the unitary matrices,

$$\Upsilon_A := \Omega_A^\dagger P_3 \Omega_A P_3 \Omega_A^\dagger, \quad \Psi_A := \Omega_A^\dagger P_3 \Omega_A P_3 \Omega_A^\dagger P_3 \Omega_A, \quad \bar{\Psi}_A := \Omega_A P_3 \Omega_A^\dagger P_3 \Omega_A P_3 \Omega_A^\dagger, \tag{3.12}$$

where $P_{\bar{3}} := \text{diag}(0, 0, 0, 1, \dots, 1)$ is a projection matrix to the vector-like families. Ψ and $\bar{\Psi}$ originate from the diagrams only with the scalars. Using Eq.(2.26), the explicit structures are given by

$$\Psi_L = \begin{pmatrix} 0 & 0 & V_{L3}^\dagger W_R Y_L^\dagger W_R \\ W_L^\dagger Y_R W_L^\dagger V_{R3} & W_L^\dagger Y_R W_L^\dagger Y_R & 0 \\ 0 & 0 & Y_L^\dagger W_R Y_L^\dagger W_R \end{pmatrix}, \quad (3.13)$$

$$\Psi_R = \begin{pmatrix} 0 & V_{R3}^\dagger W_L Y_R^\dagger W_L & 0 \\ 0 & Y_R^\dagger W_L Y_R^\dagger W_L & 0 \\ W_R^\dagger Y_L W_R^\dagger V_{L3} & 0 & W_R^\dagger Y_L W_R^\dagger Y_L \end{pmatrix}, \quad (3.14)$$

$$\bar{\Psi}_L = \begin{pmatrix} 0 & 0 & V_{3L} W_R^\dagger Y_L W_R^\dagger \\ W_L Y_R^\dagger W_L V_{3R}^\dagger & W_L Y_R^\dagger W_L Y_R^\dagger & 0 \\ 0 & 0 & Y_L W_R^\dagger Y_L W_R^\dagger \end{pmatrix}, \quad (3.15)$$

$$\bar{\Psi}_R = \begin{pmatrix} 0 & V_{3R} W_L^\dagger Y_R W_L^\dagger & 0 \\ 0 & Y_R W_L^\dagger Y_R W_L^\dagger & 0 \\ W_R Y_L^\dagger W_R V_{3L}^\dagger & 0 & W_R Y_L^\dagger W_R Y_L^\dagger \end{pmatrix}. \quad (3.16)$$

Since the top-left 3×3 blocks are zero, the flavor violating processes via these coupling structures are suppressed under the conditions (i) and (ii).

The situation is different in the diagrams involving both LQ and adjoint scalars, denoted by Υ_L and Υ_R , which are given by

$$\Upsilon_L = \begin{pmatrix} V_{L3}^\dagger W_R V_{3L}^\dagger & 0 & V_{L3}^\dagger W_R Y_L^\dagger \\ 0 & W_L^\dagger Y_R W_L^\dagger & 0 \\ Y_L^\dagger W_R V_{3L}^\dagger & 0 & Y_L^\dagger W_R Y_L^\dagger \end{pmatrix}, \quad \Upsilon_R = \begin{pmatrix} V_{R3}^\dagger W_L V_{3R}^\dagger & V_{R3}^\dagger W_L Y_R^\dagger & 0 \\ Y_R^\dagger W_L V_{3R}^\dagger & Y_R^\dagger W_L Y_R^\dagger & 0 \\ 0 & 0 & W_R^\dagger Y_L W_R^\dagger \end{pmatrix}. \quad (3.17)$$

We find that the SM top-left blocks are 3×3 unitary matrices and cannot be vanishing. Note that one of the two indices of $\Upsilon_{L,R}^{li}$ represents quark flavor and the other represents lepton flavor. Thus, even if the SM blocks in $\Upsilon_{L,R}^{li}$ are diagonal, it does not indicate that the flavor violating processes with $i \neq j$ or $k \neq l$ are vanishing. Indeed, we will see in the next section that the rapid $K_L \rightarrow \mu e$ decay is caused by taking $\Upsilon_{L,R}^{li} = \delta_{li}$.

The above results can be understood as follows. Without the $SU(2)_L$ breaking effects, the Yukawa couplings of Δ with the SM leptons $e_{L,R}$ are schematically given by

$$\Delta (\bar{e}_L Y_{e_L} E_R + \bar{\mathcal{E}}_L Y_{e_R} e_R) + h.c., \quad (3.18)$$

where E_R (\mathcal{E}_L) is the $SU(2)_L$ doublet (singlet) heavy lepton. Hence, the SM leptons with different chirality cannot participate in the same Yukawa couplings of Δ without the $SU(2)_L$ breaking effects. As a result, the non-vanishing box contributions with two scalars are proportional to

Table 2: Values of masses m_M , lifetimes τ_M and decay constants f_M of the mesons $M = K, B_d, B_s$ [38, 39].

M	m_M [GeV]	τ_M [$\times 10^{12} \cdot \text{GeV}^{-1}$]	f_M [GeV]
K	0.4976	7.773×10^4	0.1552
B_d	5.280	2.308	0.1920
B_s	5.367	2.320	0.2284

$Y_{e_L}^\dagger Y_{e_L}$ or $Y_{e_R}^\dagger Y_{e_R}$ which are diagonal under the condition (ii). Thus, those diagrams do not induce the flavor violating interaction. On the other hand, once the LQ interactions of the SM down quarks $d_{L,R}$

$$X^\mu (g_{d_L} \bar{d}_L \gamma_\mu E_L + g_{d_R} \bar{d}_R \gamma_\mu \mathcal{E}_R) + h.c., \quad (3.19)$$

are considered, the SM down-type quarks can interact with the SM charged leptons via the vector-like leptons. Such contribution has the coupling structure of $Y_{e_R} g_{d_R}$ or $Y_{e_L}^\dagger g_{d_L}$, which corresponds to $\Upsilon_{L,R}$, and hence is non-vanishing. $\Upsilon_{L,R}$ is also understood as a generalized version of $g_A \kappa_L$ in Eq. (2.10).

As a side remark, we comment on the flavor violation in four-quark and four-lepton operators. Based on our finding in this section, the unsuppressed coupling structures $\Upsilon_{L,R}$ are obtained only from the box diagrams with one LQ and one h_Δ (or Δ_8). Such diagrams only show up in the $\bar{d}_i d_j \rightarrow \bar{e}_k e_l$ processes and do not induce the four-quark and four-lepton operators. The latter operators are only generated from the box diagrams with two LQs or two h_Δ , providing the coupling structures of $\Omega_A \Omega_A^\dagger$, $\Omega_A \Omega_{\bar{A}}^\dagger$, Ψ , or $\bar{\Psi}$ which only contain flavor-conserving or vanishing elements for the SM fermions. Therefore, the flavor violations from the four-quark and four-lepton operators, such as neutral meson mixing and three-body lepton flavor violating decays $\ell \rightarrow \ell' \ell' \ell''$ ($\ell, \ell', \ell'' = e, \mu, \tau$), are suppressed under the conditions (i) and (ii).

4 Phenomenology

We evaluate the LFV processes, especially the leptonic meson decays and $\mu \rightarrow e$ conversion, assuming the condition (i) and (ii). We see that there is an upper limit on the vector-like fermion mass for a given LQ mass when experimental bounds on those processes are respected.

4.1 Flavor violating leptonic decays of neutral mesons

Rare meson decays $M_{ij} \rightarrow e_k^- e_l^+$, where M_{ij} is a meson composed of $\bar{d}_j d_i$, are the key processes induced from the semi-leptonic operators of our interest. In general, the partial decay width of $M_{ij} \rightarrow e_k^- e_l^+$ is given by

$$\Gamma(M_{ij} \rightarrow e_k^- e_l^+) = \frac{f_M^2 \beta}{16\pi m_M} [(m_M^2 - m_l^2 - m_k^2) a^{ij,kl} - b^{ij,kl}], \quad (4.1)$$

Table 3: LFV decay modes of neutral mesons. The leptonic indices (k, l) are added with its counterpart (l, k) .

observable	upper limit	$(i, j), (k, l)$	Ref.
BR $(K_L \rightarrow \mu e)$	4.7×10^{-12}	(1, 2), (1, 2)	[38]
BR $(B_d \rightarrow \mu e)$	1.0×10^{-9}	(1, 3), (1, 2)	[38]
BR $(B_d \rightarrow \tau e)$	2.8×10^{-5}	(1, 3), (1, 3)	[38]
BR $(B_d \rightarrow \tau \mu)$	1.4×10^{-5}	(1, 3), (2, 3)	[38]
BR $(B_s \rightarrow \mu e)$	5.4×10^{-9}	(2, 3), (1, 2)	[38]
BR $(B_s \rightarrow \tau e)$	-	(2, 3), (1, 3)	[38]
BR $(B_s \rightarrow \tau \mu)$	4.2×10^{-5}	(2, 3), (2, 3)	[38]

$$a^{ij,kl} = \sum_{A=L,R} \left| \bar{m}_M S_A^{ij,kl} - m_l V_A^{ij,kl} + m_k V_A^{ij,kl} \right|^2, \quad (4.2)$$

$$b^{ij,kl} = 4m_k m_l \text{Re} \left[\left(\bar{m}_M S_L^{ij,kl} - m_l V_L^{ij,kl} + m_k V_R^{ij,kl} \right) \left(\bar{m}_M S_R^{ij,kl} - m_l V_R^{ij,kl} + m_k V_L^{ij,kl} \right)^* \right], \quad (4.3)$$

$$V_A^{ij,kl} := \frac{C_{VRA}^{ij,kl} - C_{VLA}^{ij,kl}}{2}, \quad S_A^{ij,kl} := \frac{C_{SRA}^{ij,kl} - C_{SLA}^{ij,kl}}{2}, \quad (4.4)$$

where f_M and m_M are a decay constant and mass of a meson M , and

$$\beta := \sqrt{1 - 2 \frac{m_l^2 + m_k^2}{m_M^2} + \frac{(m_l^2 - m_k^2)^2}{m_M^4}}. \quad (4.5)$$

Here, we used

$$\langle 0 | \bar{d}_j \gamma^\mu \gamma_5 d_i | M_{ij} \rangle = i f_M P_M^\mu, \quad \langle 0 | \bar{d}_j \gamma_5 d_i | M_{ij} \rangle = -i f_M \bar{m}_M, \quad (4.6)$$

where P_M^μ is a four momentum of a meson M and $\bar{m}_M := m_M^2 / (m_{d_i} + m_{d_j})$ with m_{d_i} being mass of quark d_i . Since the LQ is much heavy compared to the meson, the RG corrections of the strong coupling constant are included by replacing in Eq. (4.6), [30]

$$\bar{m}_M \rightarrow \bar{m}_M R_M(m_X), \quad (4.7)$$

where

$$R_M(m_X) := R(m_M, m_c; 3) R(m_c, m_b; 4) R(m_b, m_t; 5) R(m_t, m_X; 6), \quad (4.8)$$

with

$$R(\mu_1, \mu_2; n_f) := \left(\frac{g_3(\mu_1)}{g_3(\mu_2)} \right)^{\frac{8}{11 - 2n_f/3}}. \quad (4.9)$$

Here we assume that all the new particles are much heavier than the top quark and as heavy as m_X . The branching fractions are given by

$$\text{BR}(M_{ij} \rightarrow e_k e_l) \simeq \tau_M \left\{ \Gamma(M_{ij} \rightarrow e_k^- e_l^+) + \Gamma(M_{ij} \rightarrow e_k^+ e_l^-) \right\}. \quad (4.10)$$

In our calculation, we use the values of the meson parameters and the experimental upper bounds in Tables 2 and 3, respectively.

4.2 μ - e conversion

When the quark flavor diagonal pieces in Eq.(3.7) are non-vanishing, μ - e conversion can also provide a leading constraint. The conversion rate is given by [40]

$$\Gamma_{\text{conv}} = 4m_\mu^5 \left(\left| \sum_{N=p,n} \left(\tilde{C}_{VL}^N V_N + m_N \tilde{C}_{SL}^N S_N \right) \right|^2 + \left| \sum_{N=p,n} \left(\tilde{C}_{VR}^N V_N + m_N \tilde{C}_{SR}^N S_N \right) \right|^2 \right), \quad (4.11)$$

where

$$\tilde{C}_{VL}^N = \sum_{q=u,d,s} C_{VL}^q f_{V_N}^q, \quad \tilde{C}_{SL}^N = \sum_{q=u,d,s} C_{SL}^q f_{S_N}^q + \frac{2}{27} f_G^N \sum_{Q=c,b,t} C_{SL}^Q, \quad (4.12)$$

$$\tilde{C}_{VR}^N = \sum_{q=u,d,s} C_{VR}^q f_{V_N}^q, \quad \tilde{C}_{SR}^N = \sum_{q=u,d,s} C_{SR}^q f_{S_N}^q + \frac{2}{27} f_G^N \sum_{Q=c,b,t} C_{SR}^Q. \quad (4.13)$$

The values of nucleon form factors for light quarks are collected in Table 4. The form factor for gluon is related to those for light quarks via the QCD trace anomaly, $f_G^N = 1 - \sum_{q=u,d,s} f_{S_N}^q$. We ignore the vector-like quark contributions to \tilde{C}_{SL}^N and \tilde{C}_{SR}^N through the trace anomaly since these are suppressed by the vector-like quark masses. In our model, the scalar and vector coefficients are loop-induced and given in terms of the Wilson coefficients of the semi-leptonic operators given in Eq.(3.7),

$$C_{VL}^{d_i} = \frac{1}{2}(C_{VLL}^{ii,21} + C_{VRL}^{ii,21}), \quad C_{VR}^{d_i} = \frac{1}{2}(C_{VRR}^{ii,21} + C_{VLR}^{ii,21}), \quad (4.14)$$

$$C_{SL}^{d_i} = \frac{1}{2m_{d_i}}(C_{SLR}^{ii,21} + C_{SRR}^{ii,21}), \quad C_{SR}^{d_i} = \frac{1}{2m_{d_i}}(C_{SRL}^{ii,21} + C_{SLL}^{ii,21}), \quad (4.15)$$

where the index i is not summed. The current (future) limit is set on the conversion rate per capture rate [41–44],

$$\text{BR}(\mu \rightarrow e)^{\text{Au(Al)}} = \frac{\Gamma_{\text{conv}}}{\Gamma_{\text{capt}}} < 7 \times 10^{-13} \quad (6 \times 10^{-17}). \quad (4.16)$$

Table 4: Values of vector [40] and scalar [45] nucleon form factors. The coefficients S_N, V_N where $N = p, n$ are calculated in Ref. [46]. The capture rates are given in Ref. [46, 47].

$f_{V_p}^u$	$f_{V_p}^d$	$f_{V_n}^u$	$f_{V_n}^d$	$f_{V_p}^s = f_{V_n}^s$
2	1	1	2	0
$f_{S_p}^u$	$f_{S_p}^d$	$f_{S_n}^u$	$f_{S_n}^d$	$f_{S_p}^s = f_{S_n}^s$
0.0191	0.0363	0.0171	0.0404	0.043

Target	S_p	S_n	V_p	V_n	$\Gamma_{\text{capt}} [10^6 \cdot s^{-1}]$
Au	0.0614	0.0918	0.0974	0.146	13.07
Al	0.0155	0.0167	0.0161	0.0173	0.705

4.3 Simplified analysis

We shall compare the box-induced LFV processes with the experimental limits. For concreteness, we consider $N_L = N_R = 3$ which is the minimal option to realize $X_L = X_R = 0$. We neglect the sub-dominant effects suppressed by η , and thus all flavor violating processes are induced via $\Upsilon_{L,R}^{ij}$ which corresponds to the SM blocks of $\Upsilon_{L,R}$. In this case, $\Upsilon_{L,R}^{ij}$ are 3×3 unitary matrices and are treated as free parameters in our study. We further assume that the SM down-type fermions are in the mass basis for a given $\Upsilon_{L,R}^{ij}$, i.e.

$$m_{33} \simeq \text{diag}(m_d, m_s, m_b), \quad \tilde{m}_{33} \simeq V_{L3}^\dagger m_{LR} V_{R3} \simeq \text{diag}(m_e, m_\mu, m_\tau). \quad (4.17)$$

We consider for simplicity the relations between the mass parameters

$$m_{\text{VL}} := m_E = m_D, \quad m_{h_\Delta} = m_X, \quad (4.18)$$

where the LQ mass m_X is related to v_Δ and g_4 via Eq. (2.22). In our analysis, the input parameters are thus

$$m_X, \quad m_{\text{VL}}, \quad \Upsilon_L^{ij}, \quad \Upsilon_R^{ij}. \quad (4.19)$$

and $g_4 = 1$ is fixed, which is consistent with the strong coupling constant at the TeV scale.

Among the LFV meson decays, $K_L \rightarrow \mu e$ is the most sensitive to new physics contributions. The branching fraction is given by

$$\text{BR}(K_L \rightarrow \mu e) \simeq \frac{\tau_K m_K f_K^2}{16\pi m_X^4} |C_0|^2 \left(1 - \frac{m_\mu^2}{m_K^2}\right)^2 \sum_{A=L,R} \sum_{p=1,2} |\Upsilon_A^{2p}|^2 \left| \overline{m}_K \Upsilon_A^{1\bar{p}} - \frac{m_\mu}{2} \Upsilon_A^{1\bar{p}} \right|^2, \quad (4.20)$$

where $\bar{p} = 2, 1$ for $p = 1, 2$ and the electron mass is neglected. The coefficient C_0 is defined as

$$C_0 := \frac{9m_{\text{VL}}^4}{16v_\Delta^4} \left(\frac{1}{4} G_1(m_{\text{VL}}, m_{\text{VL}}; m_X, m_X) - G_0(m_{\text{VL}}, m_{\text{VL}}; m_X, m_X) \right). \quad (4.21)$$

With the sizable chiral enhancement proportional to \bar{m}_K , we find the branching fraction to be

$$\text{BR}(K_L \rightarrow \mu e) \simeq 3.5 \times 10^{-5} \times \left| \Upsilon_A^{2p} \Upsilon_A^{1\bar{p}} \right|^2 \left(\frac{|C_0|}{1/(16\pi^2)} \right)^2 \left(\frac{5 \text{ TeV}}{m_X} \right)^4, \quad (4.22)$$

while without the chiral enhancement,

$$\text{BR}(K_L \rightarrow \mu e) \simeq 3.0 \times 10^{-9} \times \left| \Upsilon_A^{2p} \Upsilon_A^{1\bar{p}} \right|^2 \left(\frac{|C_0|}{1/(16\pi^2)} \right)^2 \left(\frac{5 \text{ TeV}}{m_X} \right)^4. \quad (4.23)$$

Hence there should be $\mathcal{O}(10^{-7})$ and $\mathcal{O}(10^{-3})$ suppression from the couplings and masses with and without the chiral enhancement, respectively. It is illuminating to give the scaling of the loop function C_0 with $m_{\text{VL}} \ll m_X$,

$$|C_0| \simeq \frac{m_{\text{VL}}^4}{8\pi^2 m_X^4} \left(\frac{7}{4} + \log \frac{m_{\text{VL}}^2}{m_X^2} \right). \quad (4.24)$$

In this limit, the branching fraction is proportional to $(m_{\text{VL}}/m_X)^8$. The mass splitting of the LQ and the vector-like fermions will help to suppress the branching fraction.

The μ - e conversion rate per capture rate on the gold target is given by

$$\text{BR}(\mu \rightarrow e)^{\text{Au}} = \frac{m_\mu^5}{\Gamma_{\text{capt}}^{\text{Au}} m_X^4} |C_0|^2 \left(\sum_{A=L,R} |\Upsilon_A^{2i}|^2 \left| \sum_{N=p,n} \sum_{i=1,2,3} \frac{1}{2} \Upsilon_A^{1i} f_{V_N}^{d_i} V_N - \frac{m_N}{m_{d_i}} \Upsilon_A^{1i} f_{S_N}^{d_i} S_N \right|^2 \right), \quad (4.25)$$

where $f_{V_N}^b = 0$ and $f_{S_N}^b = 2f_G^N/27$. In the vector-dominant case, i.e. $|\Upsilon_A^{2i} \Upsilon_A^{1i}| \ll |\Upsilon_A^{21} \Upsilon_A^{11}|$, we have

$$\text{BR}(\mu \rightarrow e)^{\text{Au}} \simeq 3.7 \times 10^{-9} \times \left(\frac{|C_0|}{1/(16\pi^2)} \right)^2 \left(\frac{5 \text{ TeV}}{m_X} \right)^4 \sum_{A=L,R} |\Upsilon_A^{21} \Upsilon_A^{11}|^2, \quad (4.26)$$

and in the scalar-dominant case, i.e. $|\Upsilon_A^{2i} \Upsilon_A^{1i}| \gg |\Upsilon_A^{21} \Upsilon_A^{11}|$,

$$\text{BR}(\mu \rightarrow e)^{\text{Au}} \sim 7 \times 10^{-7} \times \left(\frac{|C_0|}{1/(16\pi^2)} \right)^2 \left(\frac{5 \text{ TeV}}{m_X} \right)^4 \sum_{A=L,R} \left| \sum_i \Upsilon_A^{2i} \Upsilon_A^{1i} \frac{f_{S_p}^{d_i}/m_{d_i}}{f_{S_p}^d/m_d} \right|^2, \quad (4.27)$$

where $f_{S_p}^{d_i} \sim f_{S_n}^{d_i}$ is used. It should be noted that the lighter quark has larger contribution in the scalar-dominant case due in part to a factor of $1/m_{d_i}$.

We consider three simplified cases:

$$(a) \quad \Upsilon_L^{ij} = \Upsilon_R^{ij} = \delta_{ij}, \quad (b) \quad \Upsilon_L^{ij} = \begin{pmatrix} 0 & 1 & 0 \\ 0 & 0 & 1 \\ 1 & 0 & 0 \end{pmatrix}, \quad \Upsilon_R^{ij} = \begin{pmatrix} 0 & 0 & 1 \\ 0 & 1 & 0 \\ 1 & 0 & 0 \end{pmatrix}, \quad (4.28)$$

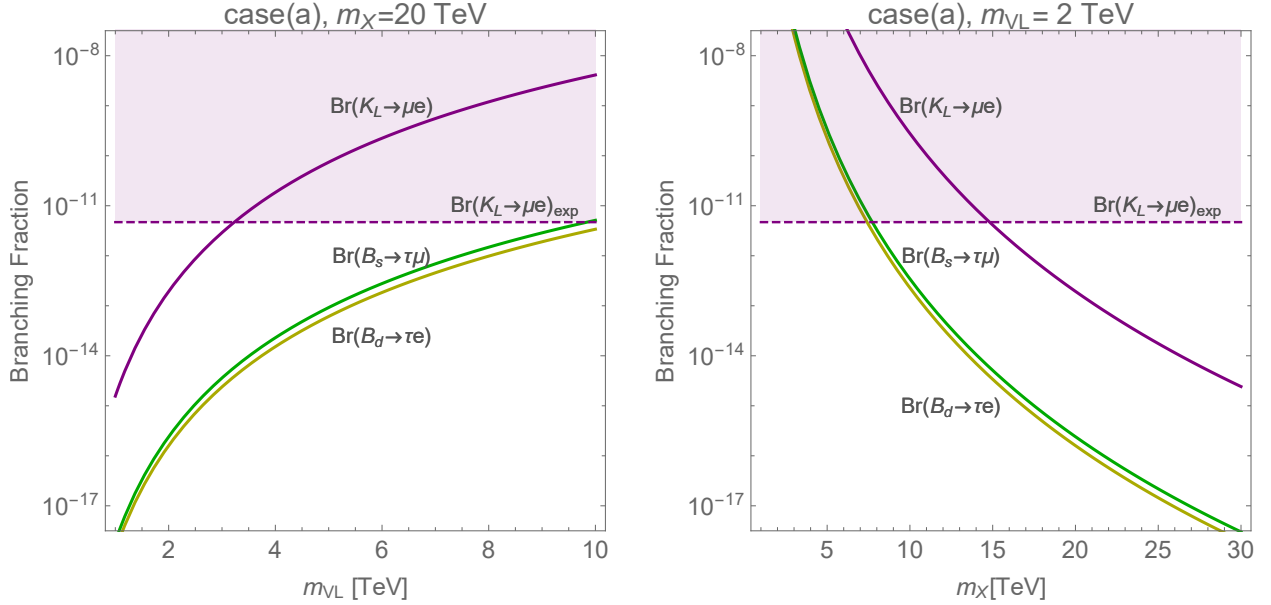


Figure 5: Values of the branching fractions in the case (a). See the main text for the detail.

and

$$(c) \quad \Upsilon_L^{ij} = \begin{pmatrix} 0 & 0 & 1 \\ 1 & 0 & 0 \\ 0 & 1 & 0 \end{pmatrix}, \quad \Upsilon_R^{ij} = \begin{pmatrix} 0 & 0 & 1 \\ 0 & 1 & 0 \\ 1 & 0 & 0 \end{pmatrix}. \quad (4.29)$$

In the case (a), there is a large contribution to $K_L \rightarrow \mu e$ via $\Upsilon_A^{11}\Upsilon_A^{22}$, while μ - e conversion is not induced because $\Upsilon_A^{2i}\Upsilon_A^{1i} = \Upsilon_A^{2i}\Upsilon_A^{1i} = 0$. In the case (b), $K_L \rightarrow \mu e$ and $B_d \rightarrow \mu e$ are not induced and, moreover, the chiral enhanced contributions to $B_s \rightarrow \mu e$ are vanishing, which suggests that the LFV meson decays only provide weak constraints. By contrast, the μ - e conversion process is induced in this case since $\Upsilon_L^{23}\Upsilon_R^{13} = \Upsilon_R^{22}\Upsilon_L^{12} = 1$. In the case (c), $K_L \rightarrow \mu e$ and $\mu \rightarrow e$ conversion are absent while $B_d, B_s \rightarrow \mu e$ are chiral enhanced. Since $K_L \rightarrow \mu e$ and $\mu \rightarrow e$ conversion give much stronger bounds than the others, the limits on the case (c) will be the weakest.

Figure 5 shows the values of the branching fractions in the case (a) as a function of m_X (m_{VL}) in the left (right) panel with $m_{VL} = 20$ TeV ($m_X = 2$ TeV). The solid lines are our predictions in this model, and the horizontal dashed lines are the experimental upper limits. Note that the other decay modes not shown in the figures are vanishing in this analysis. It follows from Fig. 5 (left) that, with $m_X = 20$ TeV, we find an upper bound on $m_{VL} \lesssim 3$ TeV from $\text{BR}(K_L \rightarrow \mu e)$, whereas $\text{BR}(B_d \rightarrow \tau\mu)$ and $\text{BR}(B_s \rightarrow \tau e)$ are much smaller than the experimental limits of $\mathcal{O}(10^{-5})$. It is remarkable that the branching fractions are suppressed by a factor of m_{VL}^4/v_Δ^4 in C_0 , providing an *upper* bound on the vector-like mass for a given LQ mass. When we instead fix the vector-like fermion mass, the LQ mass scale is limit from below. One can see in Fig. 5 (right) that the LQ mass should be heavier than 15 TeV with $m_{VL} = 2$ TeV.

Figures 6 and 7 are similar plots to Fig. 5 for the case (b) and (c), respectively. In the case (b), the values of $\text{BR}(B_d \rightarrow \tau e)$ (purple) and $\text{BR}(B_d \rightarrow \tau\mu)$ (yellow dashed) are degenerate since

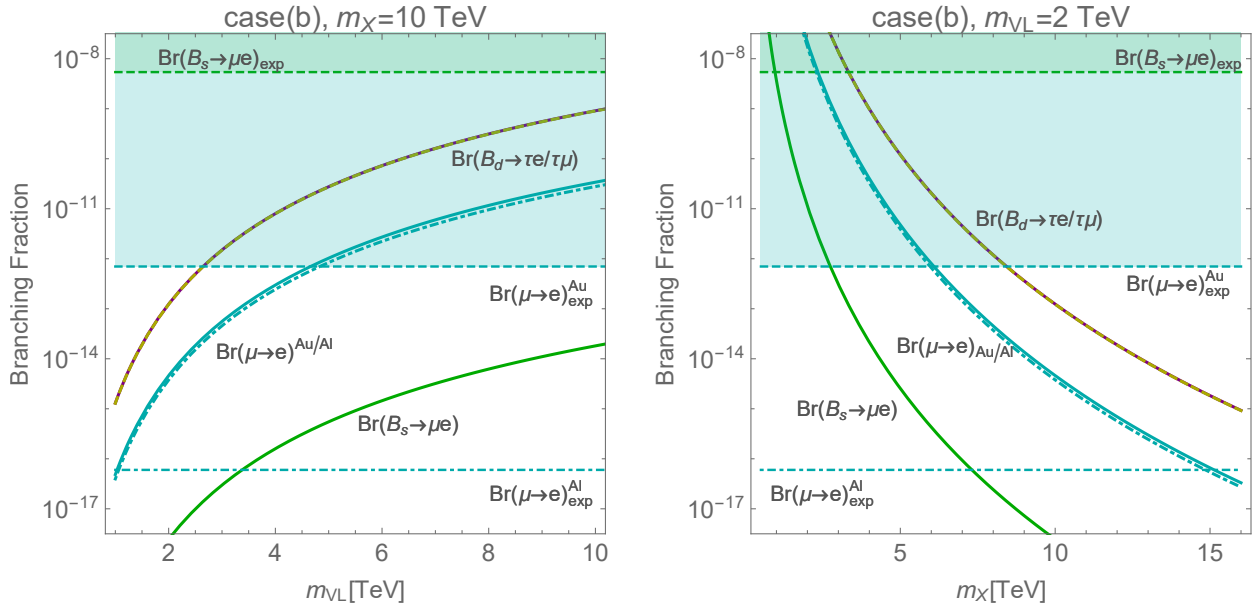


Figure 6: Values of the branching fractions in the case (b). $\text{BR}(B_d \rightarrow \tau e) \simeq \text{BR}(B_d \rightarrow \tau \mu)$ and $\text{BR}(\mu \rightarrow e)^{\text{Au}} \simeq \text{BR}(\mu \rightarrow e)^{\text{Al}}$ in this case.

the muon mass is still negligible compared to m_b and m_τ . As regards the $\mu \rightarrow e$ conversion, $\text{BR}(\mu \rightarrow e)^{\text{Au}}$ (cyan) is slightly larger than $\text{BR}(\mu \rightarrow e)^{\text{Al}}$ (cyan dashed). The horizontal dashed lines are the current upper limits on the corresponding LFV processes and the horizontal dot-dashed line is the future sensitivity to $\text{BR}(\mu \rightarrow e)^{\text{Al}}$. The $\mu \rightarrow e$ conversion provides the strongest constraint in the case (b), and it requires $m_{\text{VL}} \lesssim 4.5$ TeV for $m_X = 10$ TeV while $m_X \gtrsim 6$ TeV for $m_{\text{VL}} = 2$ TeV. The future $\text{BR}(\mu \rightarrow e)^{\text{Al}}$ measurement will improve the limits to $m_{\text{VL}} \lesssim 1$ TeV and $m_X \gtrsim 15$ TeV, respectively. We see the complementarity of LFV meson decays and the $\mu \rightarrow e$ conversion in the case (a) and (b), however, there is no contribution to both $K_L \rightarrow \mu e$ and $\mu \rightarrow e$ conversion in the case (c). The green, pink, cyan and purple lines are $\text{BR}(B_s \rightarrow \mu e)$, $\text{BR}(B_s \rightarrow \tau e)$, $\text{BR}(B_d \rightarrow \mu e)$ and $\text{BR}(B_d \rightarrow \tau e)$, respectively. The current limit reads $m_{\text{VL}} \lesssim 3$ TeV for $m_X = 5$ TeV while $m_X \gtrsim 4$ TeV for $m_{\text{VL}} = 2$ TeV. Thus 5 TeV LQ is not excluded in this case when the VL fermions are sufficiently light. This leaves the possibility of resolving the B anomalies [31].

Let us comment on the LHC constraints on the model. In our analysis, we consider the vector-like fermions to be heavier than 2 TeV which is significantly higher than the current LHC limits $m_{\text{VL}} \gtrsim 1$ TeV [48, 49]. Thus we need higher energy colliders, e.g. $\sqrt{s} = 100$ TeV to explore the allowed parameter space [50–52]. Besides, there is a model-dependent bound on the light LQ scenario, given the existence of a new neutral gauge boson Z' whose mass is correlated to the LQ mass to some extent. In fact, 2 TeV LQ is excluded by the di-muon resonance search for Z' [53], when the residual $SU(2)_R \times U(1)_{B-L}$ symmetry is broken by a scalar field with $(\overline{\mathbf{10}}, \mathbf{1}, \mathbf{3})$ under the PS symmetry [31]. Thus, additional careful consideration will be needed to achieve the LQ lighter than a few TeV.

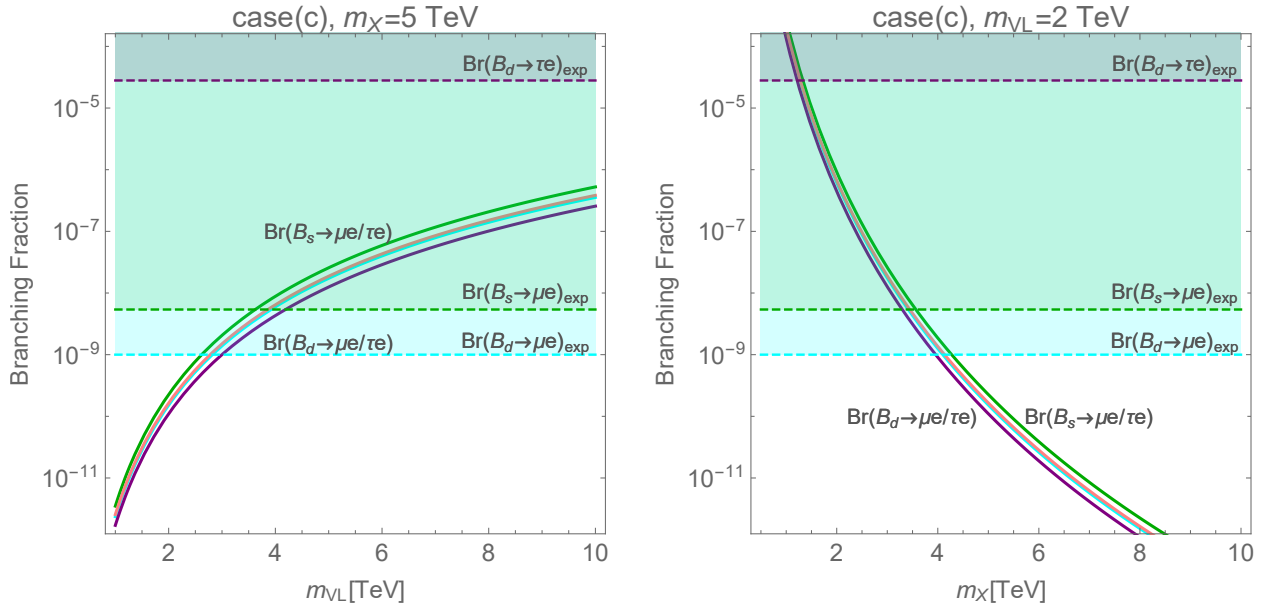


Figure 7: Values of the branching fractions in the case (c).

4.4 Comments on penguin diagrams

We comment on contributions from one-loop penguin diagrams, which may generate the flavor violation comparable with the box contributions.⁵ Figure 8 shows examples of the contributing diagrams. They fall into two categories; one violates both quark and lepton flavor and the other violates either of them but not both. The diagrams in the first and second lines of Fig. 8 belong to the first category and can generate the quark and lepton flavor violating operators in the form $(\bar{d}_j \Gamma d_i)(\bar{e}_k \Gamma e_l)$, where Γ represents an arbitrary Lorentz structure. As discussed above, such operators lead to the $K_L \rightarrow \mu e$ decay and thus to the severe constraint. These contributions, however, contain a tree-level coupling, namely $\Omega_{L,R}^{jk}$, $(\hat{Y}_\Delta^e)^{kl}$ or $(\hat{Y}_\Delta^d)^{ji}$, and are always suppressed under the condition (i).

In the second category, the lepton flavor conserving processes $\bar{d}_j d_i \rightarrow \ell \bar{\ell}$ are induced via photon and V_{B-L} penguin diagrams (the third line of Fig. 8) even though we require the condition (i). Here, let us have a closer look at the coupling structure of such contributions. In the diagrams with the LQ loop, the amplitudes of such processes contain the following structures

$$\sum_I (\Omega_{L,R})^{jI} (\Omega_{L,R}^\dagger)^{Ii} f(m_I^e, m_X), \quad \sum_I (\Omega_L)^{jI} (\Omega_R^\dagger)^{Ii} g(m_I^e, m_X), \quad (4.30)$$

where f and g are loop functions. They depend on the LQ couplings to the vector-like families. Assuming the condition (ii), the former contribution is vanishing for $i \neq j$ because of the unitarity of the LQ couplings $\Omega_{L,R}$, Eq. (3.3). The latter contribution is proportional to $(\Omega_L)^{jI} (\Omega_R^\dagger)^{Ii} \propto$

⁵There are two-loop contributions: two sets of one-loop vertex corrections involving a LQ and an adjoint scalar. However, such contributions are suppressed by the loop factor, couplings and the power of m_{VL}^2/m_X^2 and thus expected to be smaller than the one-loop box contribution.

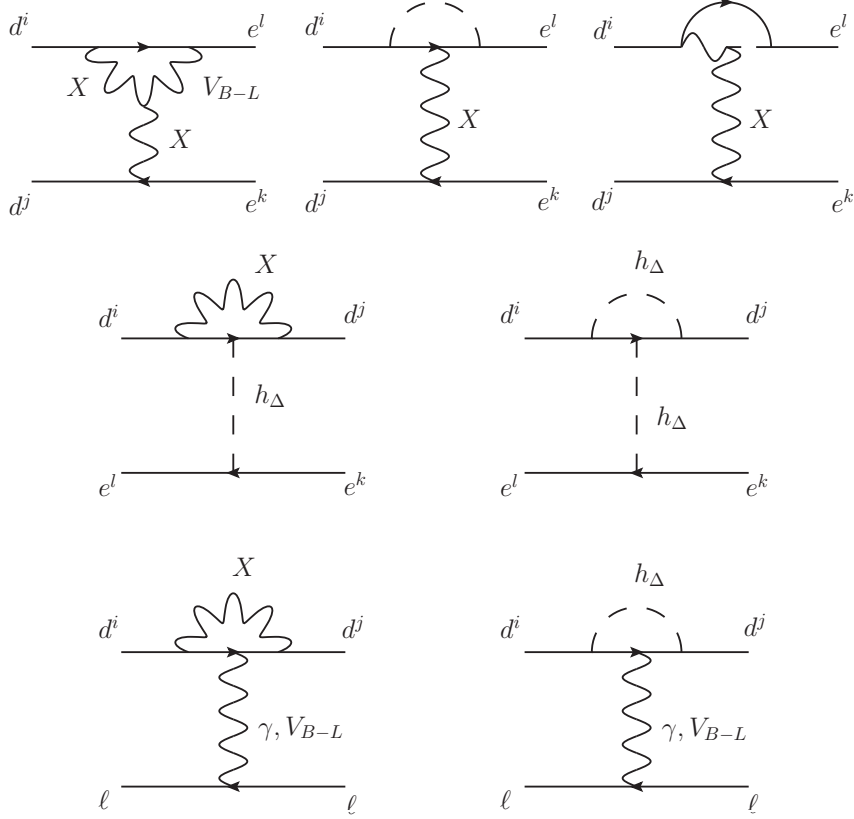


Figure 8: Example one-loop penguin contributions to semi-leptonic operators, $(\bar{d}_j \Gamma d_i)(\bar{e}_k \Gamma e_l)$ and $(\bar{d}_j \Gamma d_i)(\bar{\ell} \Gamma \ell)$.

$(\hat{Y}_\Delta^d)^{ji} + \mathcal{O}(\eta)$, and it is also vanishing. In the case of the h_Δ and Δ_8 loops, the amplitudes contain the following coupling structures

$$\sum_I (\hat{Y}_\Delta^d)^{jI} (\hat{Y}_\Delta^{d\dagger})^{Ii} f'(m_I^d, m_{h_\Delta}), \quad \sum_I (\hat{Y}_\Delta^d)^{jI} (\hat{Y}_\Delta^d)^{Ii} g'(m_I^d, m_{h_\Delta}), \quad (4.31)$$

where f' and g' are different loop functions from f and g . Under the conditions (i) and (ii), these are proportional to $\sum_I (\hat{Y}_\Delta^d)^{jI} (\hat{Y}_\Delta^{d\dagger})^{Ii} \simeq \delta^{ji}$ and $\sum_I (\hat{Y}_\Delta^d)^{jI} (\hat{Y}_\Delta^d)^{Ii} \propto (\bar{\Psi}_L)^{ji} \simeq 0$, respectively, and thus the $\bar{d}_j d_i \rightarrow \bar{\ell} \ell$ processes do not appear. Moreover, other diagrams belonging to the second category can also induce the lepton flavor violating processes, such as $\mu \rightarrow e$ conversion and $\mu \rightarrow e\gamma$, but one can readily show that these are suppressed in a similar manner. We thus conclude that the conditions (i) and (ii) are sufficient to suppress all penguin contributions in the model.

5 Summary

In this paper, we study the one-loop contributions to the flavor violating processes, especially the LFV meson decays and $\mu \rightarrow e$ conversion, in the PS model with vector-like families. These processes are known to strongly constrain the scale of the PS symmetry breaking. We clarify the conditions to suppress these processes up to at the one-loop level:

- (i) LQ couplings to the SM families are vanishing, i.e. $X_L = X_R \sim 0$,
- (ii) Masses of vector-like down-type quarks and charged leptons are individually universal,
- (iii) Υ_L and Υ_R have a certain structure such that $K_L \rightarrow \mu e$ and $\mu \rightarrow e$ conversion are sufficiently small.

These are the conditions at the leading order in $\eta := m_{\alpha\beta}/v_\Delta$.

The condition (i) is required to suppress the flavor violating processes mediated by the tree-level LQ exchange, while the one-loop box diagrams with two LQs can induce those processes only with the condition (i). Note that the tree-level flavor violations via the scalar fields are suppressed independently of the condition (i), as shown in Eqs. (2.32) and (2.33). Once we impose the condition (ii) as well as the condition (i), the flavor violating processes from the box diagrams with two LQs are suppressed due to the unitarity of the LQ gauge couplings, in analogy with the W boson coupling in the SM. We also argued that four-quarks, four-leptons and penguin operators are suppressed due to the unitarity. Therefore, the flavor violating processes like neutral meson mixing, $\mu \rightarrow e\gamma$ and $\mu \rightarrow eee$ are all suppressed under the conditions (i) and (ii).

Nonetheless, the condition (iii) is necessary to alleviate the constraints from the LFV processes induced by the box diagrams involving both vector LQ and scalars. We found that those diagrams are not suppressed even with the conditions (i) and (ii). Such contribution is well represented by a coupling structure Υ_A ($A = L, R$) defined in Eq. (3.17), whose SM blocks Υ_A^{ij} are the 3×3 unitary matrices. Because of the unitarity of Υ_A^{ij} , we cannot realize $\Upsilon_A^{ij} = 0$ and hence the flavor violation via this coupling structure is unavoidable. As a result, Υ_A^{ij} should have a structure that sufficiently suppresses the LFV processes, especially $K_L \rightarrow \mu e$ and $\mu \rightarrow e$ conversion. This is what the condition (iii) means.

To evaluate the change of the limits depending on the Υ_A^{ij} structure, we studied three simplified cases given in Eq. (4.28). In the case (a), the structure of Υ_A^{ij} allows the chiral enhanced $K_L \rightarrow \mu e$ decay, and hence $\mathcal{O}(10 \text{ TeV})$ LQ mass is required to be consistent with the experimental limit. It is remarkable that there are upper bounds on the vector-like fermion masses of $\mathcal{O}(\text{TeV})$ to respect $K_L \rightarrow \mu e$. This result would encourage direct searches for the vector-like fermions at the LHC and other future collider experiments to test this scenario. In the case (b), $K_L \rightarrow \mu e$ is not induced because of the structure of Υ_A^{ij} , but $\mu \rightarrow e$ conversion arises. The resulting lower limit on the LQ mass is 6 TeV currently and it will be improved to 15 TeV at the future experiment with the aluminum target. In the case (c), both $K_L \rightarrow \mu e$ and $\mu \rightarrow e$ conversion are absent, so $B_d \rightarrow \mu e$ gives the strongest limit. Since the experimental limits are much weaker for this decay mode, 5 TeV LQ is not excluded.

In conclusion, while we suggested the conditions (i)-(iii) to suppress the flavor violating processes, it will be interesting to study what will be caused by the violation of these conditions.

In particular, the tree-level contributions, namely the violation of the condition (i) is required to address the $R_{K^{(*)}}$ anomaly, so the full numerical analysis with both tree-level and one-loop contributions is crucial. Furthermore, this model could perhaps explain the anomaly in muon $g - 2$ via the loop diagrams involving LQ, vector-like fermions and exotic scalar particles. We leave those extended studies including the violation of three conditions for future work.

Acknowledgment

S. I. enjoys the support from the Japan Society for the Promotion of Science (JSPS) Core-to-Core Program, No.JPJSCCA20200002 and the Deutsche Forschungsgemeinschaft (DFG, German Research Foundation) under grant 396021762–TRR 257. The work of J.K. is supported in part by the Institute for Basic Science (IBS-R018-D1) and the Grant-in-Aid for Scientific Research from the Ministry of Education, Science, Sports and Culture (MEXT), Japan No. 18K13534. S.O. acknowledges financial support from the State Agency for Research of the Spanish Ministry of Science and Innovation through the “Unit of Excellence María de Maeztu 2020-2023” award to the Institute of Cosmos Sciences (CEX2019-000918-M) and from PID2019-105614GB-C21 and 2017-SGR-929 grants. The work of Y. O. is supported by Grant-in-Aid for Scientific research from the MEXT, Japan, No. 19K03867.

A Loop functions

The loop functions are shown in this appendix. First, we define

$$F_n(m_1, m_2; M_1, M_2) := \int \frac{d^4 p}{(4\pi)^4} \frac{p^{2n}}{(p^2 - m_1^2)(p^2 - m_2^2)(p^2 - M_1^2)(p^2 - M_2^2)}. \quad (\text{A.1})$$

The functions with $n = 0, 1$ are relevant to our study, which are given by

$$F_0(m_1, m_2; M_1, M_2) = \frac{-i}{16\pi^2} \frac{1}{M_1^4} \{F(x_1, x_2, \eta) + F(x_2, x_1, \eta) + F(\eta, x_1, x_2)\}, \quad (\text{A.2})$$

$$F_1(m_1, m_2; M_1, M_2) = \frac{-i}{16\pi^2} \frac{1}{M_1^2} \{x_1 F(x_1, x_2, \eta) + x_2 F(x_2, x_1, \eta) + \eta F(\eta, x_1, x_2)\}, \quad (\text{A.3})$$

where $x_1 = m_1^2/M_1^2$, $x_2 = m_2^2/M_1^2$, $\eta = M_2^2/M_1^2$. The function F is defined as

$$F(x_1, x_2, \eta) = \frac{x_1 \ln x_1}{(x_1 - 1)(x_1 - x_2)(x_1 - \eta)}. \quad (\text{A.4})$$

In the simplified analysis in Sec. 4, we consider the case of $m := m_1 = m_2$ and $M := M_1 = M_2$. In this case, F_0 and F_1 take the simplified forms,

$$F_0(m, M) = \frac{-i}{16\pi^2 M^4} \frac{2(1-x) + (1+x) \log x}{(1-x)^3}, \quad (\text{A.5})$$

$$F_1(m, M) = \frac{-i}{16\pi^2 M^2} \frac{1-x^2 + 2x \log x}{(1-x)^3}, \quad (\text{A.6})$$

where $x := m^2/M^2$. The dimensionless functions G_n are defined as the linear combinations of F_0 and F_1 ,

$$m_X^{2n-4}G_n(m_E, m_D; m_X, m_{h_\Delta}) := \frac{3}{8}F_n(m_E, m_E; m_X, m_{h_\Delta}) + \frac{11}{8}F_n(m_D, m_D; m_X, m_{h_\Delta}) + \frac{1}{4}F_n(m_E, m_D; m_X, m_{h_\Delta}). \quad (\text{A.7})$$

We also define $\tilde{F}_0(m_E, m_D; m_X, m_{h_\Delta}) := m_X^4 F_0(m_E, m_D; m_X, m_{h_\Delta})$, where \tilde{F}_0 is a dimensionless function.

B Tree-level constraints

The tree-level LQ exchange induces the LFV processes. In particular, $e-\mu$ flavor violating phenomena strongly constrain the coupling products involving the first two generations. The prime constraints arise from the LFV meson decays, especially $K_L \rightarrow \mu e$. The $\mu-e$ conversion process also brings a stringent constraint on the quark-flavor-diagonal coupling products. In order to avoid the experimental constraints, those couplings need to be smaller than $\mathcal{O}(10^{-2\sim 3})$, assuming that all the couplings have a comparable size. See Table 5, where we fix $m_X = 5 \text{ TeV}$. Furthermore one-loop induced $\mu \rightarrow e\gamma$ can constrain the coupling products. It however depends on the LQ couplings to the vector-like quarks [31], so we do not discuss it further. For the more generic analysis readers are referred to Ref. [54].

Table 5: The upper limit on the coupling products from the $\mu-e$ flavor violating processes.

coupling product	upper limit	process	bound
$(\hat{g}_{d_L}^X)_{de} (\hat{g}_{d_R}^X)_{s\mu}, (\hat{g}_{d_R}^X)_{de} (\hat{g}_{d_L}^X)_{s\mu}$	$\lesssim 10^{-5}$	$K_L \rightarrow \mu e$	[38]
$(\hat{g}_{d_L}^X)_{se} (\hat{g}_{d_R}^X)_{d\mu}, (\hat{g}_{d_R}^X)_{se} (\hat{g}_{d_L}^X)_{d\mu}$	$\lesssim 10^{-5}$	$K_L \rightarrow \mu e$	[38]
$(\hat{g}_{d_L}^X)_{de} (\hat{g}_{d_L}^X)_{d\mu}$	$\lesssim 10^{-4}$	$\mu-e$ conversion	[41]
$(\hat{g}_{d_R}^X)_{de} (\hat{g}_{d_R}^X)_{d\mu}$	$\lesssim 10^{-5}$	$\mu-e$ conversion	[41]
$(\hat{g}_{d_L}^X)_{de} (\hat{g}_{d_R}^X)_{d\mu}$	$\lesssim 10^{-5}$	$\mu-e$ conversion	[41]
$(\hat{g}_{d_L}^X)_{se} (\hat{g}_{d_R}^X)_{s\mu}$	$\lesssim 10^{-5}$	$\mu-e$ conversion	[41]

The h_Δ and Δ_8 exchanging also contributes to the flavor violating processes. The scalar couplings with the SM fermions are generally flavor violating and linear to

$$(\hat{g}_{d_L}^X)_{iD} m_D^e (\hat{g}_{d_R}^X)_{Dj}^\dagger, (\hat{g}_{d_L}^X)_{iD}^\dagger m_D^d (\hat{g}_{d_R}^X)_{Dj}. \quad (\text{B.1})$$

As we see in the main text, the scalar couplings are related to the LQ couplings involving heavy fermions as well as SM fermions. Taking into account the tree-level exchanging of h_Δ and Δ_8

and fixing $m_{h_\Delta} = m_{\Delta_8} = 5 \text{ TeV}$, we can also derive the experimental constraints on the scalar couplings

$$\frac{1}{3}\sqrt{\frac{3}{8}} \left(|\hat{Y}_{\Delta ij}^d| \right) \leq \begin{pmatrix} 5 \times 10^{-3} & 10^{-5} & 10^{-3} \\ 10^{-5} & 1 \times 10^{-2} & 5 \times 10^{-3} \\ 10^{-3} & 5 \times 10^{-3} & 1 \end{pmatrix}, \quad (\text{B.2})$$

$$\sqrt{\frac{3}{8}} \left(|\hat{Y}_{\Delta ij}^e| \right) \leq \begin{pmatrix} 1 & 1 \times 10^{-3} & 0.5 \\ 1 \times 10^{-3} & 1 & 0.5 \\ 0.5 & 0.5 & 1 \end{pmatrix}. \quad (\text{B.3})$$

The upper bounds on the off-diagonal elements of $(\hat{Y}_{\Delta}^d)_{ij}$ are estimated using $K-\bar{K}$, $B-\bar{B}$ and $B_s-\bar{B}_s$ mixings. The bounds on the off-diagonal elements of $(\hat{Y}_{\Delta}^e)_{ij}$ are derived from $\mu \rightarrow 3e$, $\tau \rightarrow \ell\ell'$, by setting all diagonal elements to unity. The bounds on the diagonal elements of $(\hat{Y}_{\Delta}^d)_{ij}$ are derived from the μ - e conversion with the maximally allowed $(\hat{Y}_{\Delta}^e)_{e\mu}$. As discussed in the main text, the conditions (i) and (ii) suppress those dangerous couplings.

References

- [1] J. C. Pati and A. Salam, *Lepton Number as the Fourth Color*, *Phys. Rev. D* **10** (1974) 275–289.
- [2] LHCb collaboration, R. Aaij et al., *Measurement of Form-Factor-Independent Observables in the Decay $B^0 \rightarrow K^{*0}\mu^+\mu^-$* , *Phys. Rev. Lett.* **111** (2013) 191801, [[1308.1707](#)].
- [3] LHCb collaboration, R. Aaij et al., *Test of lepton universality with $B^0 \rightarrow K^{*0}\ell^+\ell^-$ decays*, *JHEP* **08** (2017) 055, [[1705.05802](#)].
- [4] LHCb collaboration, R. Aaij et al., *Test of lepton universality using $B^+ \rightarrow K^+\ell^+\ell^-$ decays*, *Phys. Rev. Lett.* **113** (2014) 151601, [[1406.6482](#)].
- [5] LHCb collaboration, R. Aaij et al., *Search for lepton-universality violation in $B^+ \rightarrow K^+\ell^+\ell^-$ decays*, *Phys. Rev. Lett.* **122** (2019) 191801, [[1903.09252](#)].
- [6] LHCb collaboration, R. Aaij et al., *Angular analysis of the $B^0 \rightarrow K^{*0}\mu^+\mu^-$ decay using 3 fb^{-1} of integrated luminosity*, *JHEP* **02** (2016) 104, [[1512.04442](#)].
- [7] LHCb collaboration, R. Aaij et al., *Measurement of CP-Averaged Observables in the $B^0 \rightarrow K^{*0}\mu^+\mu^-$ Decay*, *Phys. Rev. Lett.* **125** (2020) 011802, [[2003.04831](#)].
- [8] LHCb collaboration, R. Aaij et al., *Angular Analysis of the $B^+ \rightarrow K^{*+}\mu^+\mu^-$ Decay*, *Phys. Rev. Lett.* **126** (2021) 161802, [[2012.13241](#)].
- [9] LHCb collaboration, R. Aaij et al., *Tests of lepton universality using $B^0 \rightarrow K_S^0\ell^+\ell^-$ and $B^+ \rightarrow K^{*+}\ell^+\ell^-$ decays*, [2110.09501](#).

- [10] G. Isidori, S. Nabeebaccus and R. Zwicky, *QED corrections in $\bar{B} \rightarrow \bar{K} \ell^+ \ell^-$ at the double-differential level*, *JHEP* **12** (2020) 104, [[2009.00929](#)].
- [11] BABAR collaboration, J. Lees et al., *Evidence for an excess of $\bar{B} \rightarrow D^{(*)} \tau^- \bar{\nu}_\tau$ decays*, *Phys. Rev. Lett.* **109** (2012) 101802, [[1205.5442](#)].
- [12] BABAR collaboration, J. Lees et al., *Measurement of an Excess of $\bar{B} \rightarrow D^{(*)} \tau^- \bar{\nu}_\tau$ Decays and Implications for Charged Higgs Bosons*, *Phys. Rev. D* **88** (2013) 072012, [[1303.0571](#)].
- [13] BELLE collaboration, M. Huschle et al., *Measurement of the branching ratio of $\bar{B} \rightarrow D^{(*)} \tau^- \bar{\nu}_\tau$ relative to $\bar{B} \rightarrow D^{(*)} \ell^- \bar{\nu}_\ell$ decays with hadronic tagging at Belle*, *Phys. Rev. D* **92** (2015) 072014, [[1507.03233](#)].
- [14] BELLE collaboration, Y. Sato et al., *Measurement of the branching ratio of $\bar{B}^0 \rightarrow D^{*+} \tau^- \bar{\nu}_\tau$ relative to $\bar{B}^0 \rightarrow D^{*+} \ell^- \bar{\nu}_\ell$ decays with a semileptonic tagging method*, *Phys. Rev. D* **94** (2016) 072007, [[1607.07923](#)].
- [15] BELLE collaboration, S. Hirose et al., *Measurement of the τ lepton polarization and $R(D^*)$ in the decay $\bar{B} \rightarrow D^* \tau^- \bar{\nu}_\tau$* , *Phys. Rev. Lett.* **118** (2017) 211801, [[1612.00529](#)].
- [16] BELLE collaboration, A. Abdesselam et al., *Measurement of $\mathcal{R}(D)$ and $\mathcal{R}(D^*)$ with a semileptonic tagging method*, [[1904.08794](#)].
- [17] LHCb collaboration, R. Aaij et al., *Measurement of the ratio of branching fractions $\mathcal{B}(\bar{B}^0 \rightarrow D^{*+} \tau^- \bar{\nu}_\tau) / \mathcal{B}(\bar{B}^0 \rightarrow D^{*+} \mu^- \bar{\nu}_\mu)$* , *Phys. Rev. Lett.* **115** (2015) 111803, [[1506.08614](#)].
- [18] LHCb collaboration, R. Aaij et al., *Test of Lepton Flavor Universality by the measurement of the $B^0 \rightarrow D^{*-} \tau^+ \nu_\tau$ branching fraction using three-prong τ decays*, *Phys. Rev. D* **97** (2018) 072013, [[1711.02505](#)].
- [19] S. Iguro and R. Watanabe, *Bayesian fit analysis to full distribution data of $\bar{B} \rightarrow D^{(*)} \ell \bar{\nu} : |V_{cb}|$ determination and new physics constraints*, *JHEP* **08** (2020) 006, [[2004.10208](#)].
- [20] Y. Aoki et al., *FLAG Review 2021*, [[2111.09849](#)].
- [21] MUON G-2 collaboration, G. W. Bennett et al., *Final Report of the Muon E821 Anomalous Magnetic Moment Measurement at BNL*, *Phys. Rev. D* **73** (2006) 072003, [[hep-ex/0602035](#)].
- [22] MUON G-2 collaboration, B. Abi et al., *Measurement of the Positive Muon Anomalous Magnetic Moment to 0.46 ppm*, *Phys. Rev. Lett.* **126** (2021) 141801, [[2104.03281](#)].
- [23] T. Aoyama et al., *The anomalous magnetic moment of the muon in the Standard Model*, *Phys. Rept.* **887** (2020) 1–166, [[2006.04822](#)].
- [24] F. S. Queiroz and W. Shepherd, *New Physics Contributions to the Muon Anomalous Magnetic Moment: A Numerical Code*, *Phys. Rev. D* **89** (2014) 095024, [[1403.2309](#)].

- [25] C. Biggio, M. Bordone, L. Di Luzio and G. Ridolfi, *Massive vectors and loop observables: the $g - 2$ case*, *JHEP* **10** (2016) 002, [[1607.07621](#)].
- [26] S. M. Bilenky and S. T. Petcov, *Massive Neutrinos and Neutrino Oscillations*, *Rev. Mod. Phys.* **59** (1987) 671.
- [27] P. Hung, A. Buras and J. Bjorken, *Petite Unification of Quarks and Leptons*, *Phys. Rev. D* **25** (1982) 805.
- [28] G. Valencia and S. Willenbrock, *Quark - lepton unification and rare meson decays*, *Phys. Rev. D* **50** (1994) 6843–6848, [[hep-ph/9409201](#)].
- [29] L. Calibbi, A. Crivellin and T. Li, *Model of vector leptoquarks in view of the B-physics anomalies*, *Phys. Rev. D* **98** (2018) 115002, [[1709.00692](#)].
- [30] M. J. Dolan, T. P. Dutka and R. R. Volkas, *Lowering the scale of Pati-Salam breaking through seesaw mixing*, *JHEP* **05** (2021) 199, [[2012.05976](#)].
- [31] S. Iguro, J. Kawamura, S. Okawa and Y. Omura, *TeV-scale vector leptoquark from Pati-Salam unification with vectorlike families*, *Phys. Rev. D* **104** (2021) 075008, [[2103.11889](#)].
- [32] L. Di Luzio, J. Fuentes-Martin, A. Greljo, M. Nardecchia and S. Renner, *Maximal Flavour Violation: a Cabibbo mechanism for leptoquarks*, *JHEP* **11** (2018) 081, [[1808.00942](#)].
- [33] J. Fuentes-Martín, G. Isidori, M. König and N. Selimović, *Vector Leptoquarks Beyond Tree Level III: Vector-like Fermions and Flavor-Changing Transitions*, *Phys. Rev. D* **102** (2020) 115015, [[2009.11296](#)].
- [34] M. Blanke and A. Crivellin, *B Meson Anomalies in a Pati-Salam Model within the Randall-Sundrum Background*, *Phys. Rev. Lett.* **121** (2018) 011801, [[1801.07256](#)].
- [35] D. Marzocca, *Addressing the B-physics anomalies in a fundamental Composite Higgs Model*, *JHEP* **07** (2018) 121, [[1803.10972](#)].
- [36] A. Crivellin, C. Greub, D. Müller and F. Saturnino, *Importance of Loop Effects in Explaining the Accumulated Evidence for New Physics in B Decays with a Vector Leptoquark*, *Phys. Rev. Lett.* **122** (2019) 011805, [[1807.02068](#)].
- [37] S. L. Glashow, J. Iliopoulos and L. Maiani, *Weak Interactions with Lepton-Hadron Symmetry*, *Phys. Rev. D* **2** (1970) 1285–1292.
- [38] PARTICLE DATA GROUP collaboration, P. Zyla et al., *Review of Particle Physics*, *PTEP* **2020** (2020) 083C01.
- [39] FLAVOUR LATTICE AVERAGING GROUP collaboration, S. Aoki et al., *FLAG Review 2019: Flavour Lattice Averaging Group (FLAG)*, *Eur. Phys. J. C* **80** (2020) 113, [[1902.08191](#)].

- [40] V. Cirigliano, R. Kitano, Y. Okada and P. Tuzon, *On the model discriminating power of $\mu \rightarrow e$ conversion in nuclei*, *Phys. Rev. D* **80** (2009) 013002, [[0904.0957](#)].
- [41] SINDRUM II collaboration, W. H. Bertl et al., *A Search for muon to electron conversion in muonic gold*, *Eur. Phys. J. C* **47** (2006) 337–346.
- [42] DEEME collaboration, H. Natori, *DeeMe experiment - An experimental search for a μ - e conversion reaction at J-PARC MLF*, *Nucl. Phys. B Proc. Suppl.* **248-250** (2014) 52–57.
- [43] COMET collaboration, Y. Kuno, *A search for muon-to-electron conversion at J-PARC: The COMET experiment*, *PTEP* **2013** (2013) 022C01.
- [44] MU2E collaboration, R. J. Abrams et al., *Mu2e Conceptual Design Report*, [1211.7019](#).
- [45] P. Junnarkar and A. Walker-Loud, *Scalar strange content of the nucleon from lattice QCD*, *Phys. Rev. D* **87** (2013) 114510, [[1301.1114](#)].
- [46] R. Kitano, M. Koike and Y. Okada, *Detailed calculation of lepton flavor violating muon electron conversion rate for various nuclei*, *Phys. Rev. D* **66** (2002) 096002, [[hep-ph/0203110](#)].
- [47] T. Suzuki, D. F. Measday and J. Roalsvig, *Total Nuclear Capture Rates for Negative Muons*, *Phys. Rev. C* **35** (1987) 2212.
- [48] ATLAS collaboration, M. Aaboud et al., *Search for large missing transverse momentum in association with one top-quark in proton-proton collisions at $\sqrt{s} = 13$ TeV with the ATLAS detector*, *JHEP* **05** (2019) 041, [[1812.09743](#)].
- [49] CMS collaboration, A. M. Sirunyan et al., *Search for electroweak production of a vector-like T quark using fully hadronic final states*, *JHEP* **01** (2020) 036, [[1909.04721](#)].
- [50] W. Altmannshofer, M. Bauer and M. Carena, *Exotic Leptons: Higgs, Flavor and Collider Phenomenology*, *JHEP* **01** (2014) 060, [[1308.1987](#)].
- [51] P. N. Bhattiprolu and S. P. Martin, *Prospects for vectorlike leptons at future proton-proton colliders*, *Phys. Rev. D* **100** (2019) 015033, [[1905.00498](#)].
- [52] G. Guedes and J. Santiago, *New leptons with exotic decays: collider limits and dark matter complementarity*, *JHEP* **01** (2022) 111, [[2107.03429](#)].
- [53] ATLAS collaboration, G. Aad et al., *Search for high-mass dilepton resonances using 139 fb^{-1} of pp collision data collected at $\sqrt{s} = 13$ TeV with the ATLAS detector*, *Phys. Lett. B* **796** (2019) 68–87, [[1903.06248](#)].
- [54] B. Fornal, S. A. Gadam and B. Grinstein, *Left-Right $SU(4)$ Vector Leptoquark Model for Flavor Anomalies*, *Phys. Rev. D* **99** (2019) 055025, [[1812.01603](#)].